nature chemistry

ARTICLES

https://doi.org/10.1038/s41557-022-00946-9

Check for updates

O-GlcNAcylation modulates liquid–liquid phase separation of SynGAP/PSD-95

Pinou Lv[1,2,3,11], Yifei Du[1,2,3,11], Changdong He[4,5,11], Luxin Peng[1,3], Xinyue Zhou[1,2,3], Yi Wan[1,2,3], Menglong Zeng[6], Wen Zhou[1,3], Peng Zou[1,2,3,7,8], Chenjian Li[2,9], Mingjie Zhang[6,10], Suwei Dong[4,5] ✉ and Xing Chen[1,2,3,7,8] ✉

Liquid–liquid phase separation (LLPS) of SynGAP and PSD-95, two abundant proteins that interact in the postsynaptic density (PSD) of neurons, has been implicated in modulating SynGAP PSD enrichment in excitatory synapses. However, the underlying regulatory mechanisms remain enigmatic. Here we report that *O*-GlcNAcylation of SynGAP acts as a suppressor of LLPS of the SynGAP/PSD-95 complex. We identified multiple *O*-GlcNAc modification sites for the endogenous SynGAP isolated from rat brain and the recombinantly expressed protein. Protein semisynthesis was used to generate site-specifically *O*-GlcNAcylated forms of SynGAP, and in vitro and cell-based LLPS assays demonstrated that T1306 *O*-GlcNAc of SynGAP blocks the interaction with PSD-95, thus inhibiting LLPS. Furthermore, *O*-GlcNAcylation suppresses SynGAP/PSD-95 LLPS in a dominant-negative manner, enabling sub-stoichiometric *O*-GlcNAcylation to exert effective regulation. We also showed that *O*-GlcNAc-dependent LLPS is reversibly regulated by *O*-GlcNAc transferase (OGT) and *O*-GlcNAcase (OGA). These findings demonstrate that OGT- and OGA-catalysed *O*-GlcNAc cycling may serve as an LLPS-regulating post-translational modification.

In addition to the classical membrane-enclosed organelles, such as the nucleus and endoplasmic reticulum, eukaryotic cells also harbour various cellular compartments that lack membranes or are not fully enclosed by membranes for organizing the intracellular space and biochemical reactions[1–3].

Many of the membraneless organelles (for example, the nucleolus and stress granule) and membrane-semi-enclosed compartments such as the postsynaptic density (PSD) exhibit liquid-like features. These biomolecular condensates are often formed through liquid–liquid phase separation (LLPS) of proteins and/or RNA. LLPS can be driven by multivalent intermolecular interactions between folded protein domains, intrinsically disordered regions (IDRs), and RNA and proteins[2]. Although extensive efforts have been made to discover biomolecular condensates formed by LLPS and their physiological and pathological implications, the underlying regulatory mechanisms for LLPS have just begun to be unveiled[4,5].

Protein post-translational modifications (PTMs) are well poised to regulate the dynamic process of LLPS, because intermolecular interactions can be weakened or enhanced via modifications of key residues[6]. For example, arginine methylation weakens cation–π interactions of Arg with aromatic amino acids like Tyr, thus suppressing LLPS of Ddx4, hnRNPA2, FUS and FMRP[7–11]. By altering the charge of modified residues including Ser, Thr and Tyr, phosphorylation can either suppress LLPS of FUS and TDP-43 or promote LLPS of Tau and FMRP[11–14]. Interestingly, LLPS of the FMRP–CAPRIN complex is promoted by phosphorylation of either protein, but suppressed by phosphorylation of both proteins[15]. In addition, phosphorylation of the RNA polymerase II (Pol II) C-terminal domain regulates the transfer of Pol II between condensates involved in transcription initiation and RNA splicing[16].

Enlightened by the increasing importance of PTMs in regulating LLPS, we turned our attention to another type of PTM, *O*-GlcNAcylation, a simple and widespread form of protein glycosylation that occurs intracellularly[17]. An *N*-acetylglucosamine (GlcNAc) is β-*O*-linked to Ser and Thr residues by *O*-GlcNAc transferase (OGT) using uridine diphosphate (UDP)-GlcNAc as the sugar donor; *O*-GlcNAcase (OGA) catalyses the removal of O-GlcNAc from proteins. *O*-GlcNAc is highly abundant in the brain[18]. In neurons, OGT has been shown to be enriched in the PSD of excitatory synapses[19]. Various synaptic proteins are identified as *O*-GlcNAc-modified, among which is SynGAP, with multiple *O*-GlcNAcylation sites identified (Supplementary Table 1)[20]. With four C-terminal splice isoforms (SynGAP-α1, SynGAP-α2, SynGAP-β and SynGAP-γ)[21], SynGAP is one of the most abundant PSD proteins and has GTPase activating protein (GAP) activity[22]. SynGAP-α1 forms a complex with PSD-95, one of the central scaffolding proteins in PSD, through specific binding between the SynGAP PDZ-binding motif (PBM) and PSD-95 PDZ3 domain (Fig. 1a)[23–25]. This complex formation induces LLPS, which is postulated to drive PSD formation in excitatory synapses[25]. It remains unknown whether *O*-GlcNAcylation regulates LLPS of the SynGAP/PSD-95 complex.

In this Article we report the discovery of *O*-GlcNAc as a regulator of LLPS of SynGAP/PSD-95. SynGAP is identified to be *O*-GlcNAc-modified at multiple sites. To elucidate the function of *O*-GlcNAcylation at particular modification sites, we employ

[1]College of Chemistry and Molecular Engineering, Peking University, Beijing, China. [2]Peking-Tsinghua Center for Life Sciences, Peking University, Beijing, China. [3]Beijing National Laboratory for Molecular Sciences, Peking University, Beijing, China. [4]State Key Laboratory of Natural and Biomimetic Drugs, Peking University, Beijing, China. [5]School of Pharmaceutical Sciences, Peking University, Beijing, China. [6]Division of Life Science, State Key Laboratory of Molecular Neuroscience, Hong Kong University of Science and Technology, Hong Kong, China. [7]Synthetic and Functional Biomolecules Center, Peking University, Beijing, China. [8]Key Laboratory of Bioorganic Chemistry and Molecular Engineering of Ministry of Education, Peking University, Beijing, China. [9]School of Life Sciences, Peking University, Beijing, China. [10]School of Life Sciences, Southern University of Science and Technology, Shenzhen, China. [11]These authors contributed equally: Pinou Lv, Yifei Du, Changdong He. ✉e-mail: dongsw@pku.edu.cn; xingchen@pku.edu.cn

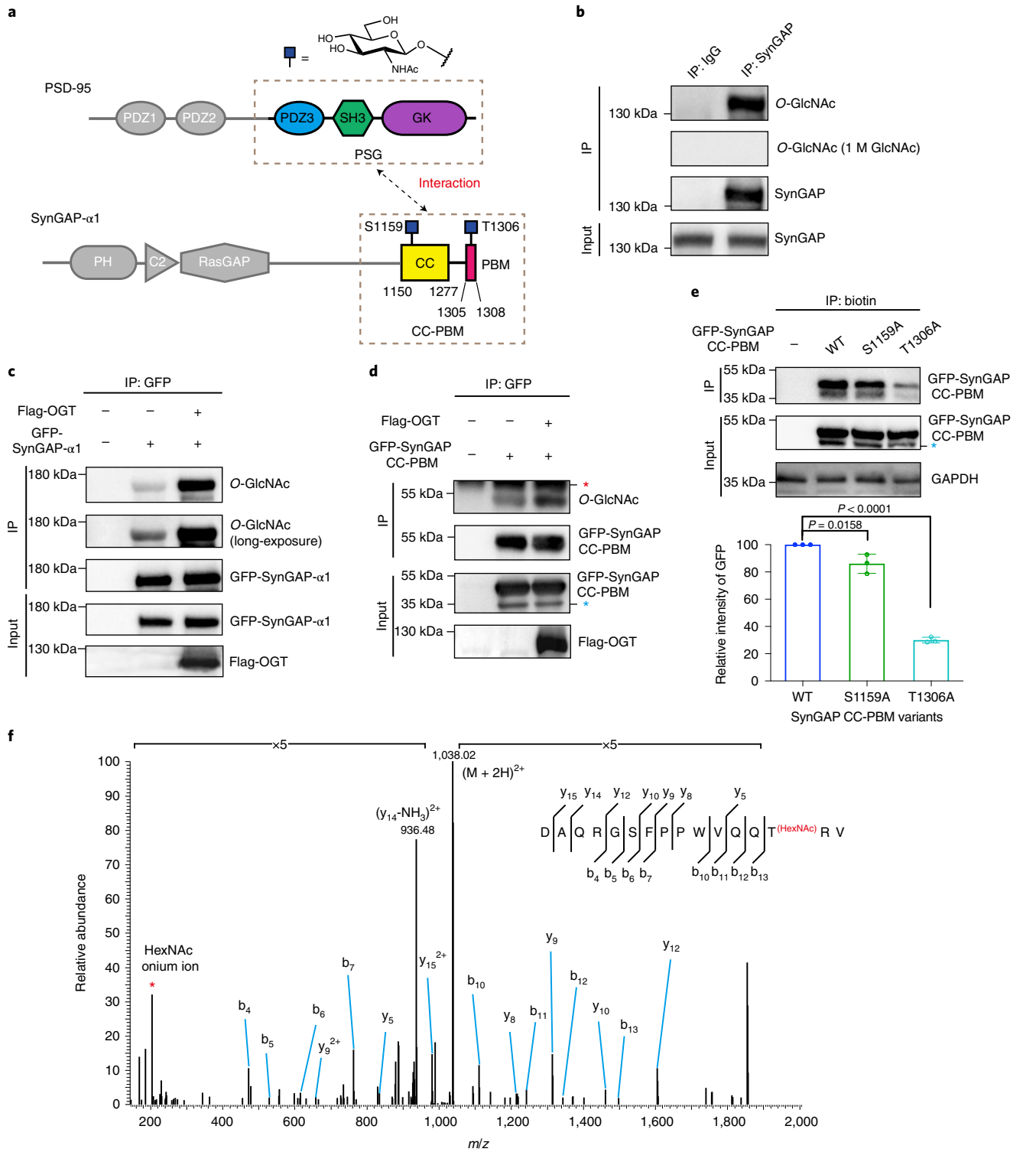

Fig. 1 | SynGAP is *O*-GlcNAcylated. a, Schematic showing the domain organization of PSD-95 and SynGAP-α1. The dashed arrow indicates interacting domains. Two *O*-GlcNAcylation sites of SynGAP are shown. **b**, Immunoblots showing endogenous SynGAP isolated from the rat brain. CTD110.6 is an *O*-GlcNAc-specific antibody. Pre-treatment with 1 M GlcNAc was used to block CTD110.6. **c**,**d**, Immunoblots showing recombinant GFP-SynGAP-α1 (**c**) or GFP-SynGAP CC-PBM (**d**) from HEK293T cells with or without co-expression of Flag-OGT. The red and blue asterisks indicate bands of the IgG heavy chain and the non-specifically degraded GFP-SynGAP CC-PBM, respectively. **e**, Immunoblots (top) showing the *O*-GlcNAcylation levels of recombinant GFP-SynGAP CC-PBM and the T1306A and S1159A mutants from HEK293T cells. The *O*-GlcNAcylated proteins in lysates were chemoenzymatically labelled with biotin and immunoprecipitated with streptavidin beads. Bar graph (bottom) showing relative *O*-GlcNAcylation levels, normalized to that of WT GFP-SynGAP CC-PBM. Error bars represent mean ± s.d. Differences were assessed by one-way analysis of variance (ANOVA) followed by Tukey's multiple comparisons test with 95% confidence interval (CI); $P < 0.05$ is considered significant. The blue asterisk indicates bands of the non-specifically degraded protein. **f**, HCD-MS/MS spectrum of an *O*-GlcNAcylated peptide of endogenous SynGAP-α1 from the rat brain. The matched fragment ions are marked. The y_5 and b_{13} ions unambiguously confirm *O*-GlcNAcylation at T1306. In **b**–**e**, representative results are shown from three independent experiments.

the protein semisynthesis strategy to generate site-specifically *O*-GlcNAcylated SynGAP proteins. In vitro assays using the synthetic proteins demonstrate that T1306 *O*-GlcNAc of SynGAP blocks its interaction with PSD-95, thus inhibiting LLPS. The inhibitory function of SynGAP T1306 *O*-GlcNAc is confirmed in living cells. More importantly, *O*-GlcNAcylation suppresses SynGAP/PSD-95 LLPS in a dominant-negative manner, which enables the sub-stoichiometric *O*-GlcNAcylation to effectively exert the regulatory function. Finally, we show that the *O*-GlcNAc-dependent LLPS is reversibly regulated by OGT and OGA.

Results

SynGAP is *O*-GlcNAcylated in the CC-PBM domain. We first isolated endogenous SynGAP from the rat brain by immunoprecipitation using an anti-SynGAP antibody and validated its *O*-GlcNAcylation by immunoblotting using an *O*-GlcNAc-recognizing antibody (Fig. 1b). Furthermore, the green fluorescent protein (GFP)-tagged rat SynGAP-α1 was *O*-GlcNAcylated by OGT when recombinantly expressed in HEK293T cells, and overexpression of OGT increased the modification level (Fig. 1c and Extended Data Fig. 1a). Mass spectrometry (MS) analysis of GFP-SynGAP-α1 purified from the OGT-overexpressed cells identified 21 modification sites, 11 of which were newly identified (Supplementary Table 2).

The complex formed by the C terminus of SynGAP-α1 (A1150-V1308) containing the coiled-coil (CC) domain and PBM (referred to as SynGAP CC-PBM; Fig. 1a) and the PDZ3-SH3-GK tandem at the C terminus of PSD-95 (referred to as PSD-95 PSG; Fig. 1a) was shown to co-phase separate both in vitro and in live cells[25]. Two of the *O*-GlcNAcylation sites identified from GFP-SynGAP-α1 (Ser1159 and Thr1306) are located within the SynGAP CC-PBM (Fig. 1a). We therefore confirmed that the GFP-SynGAP CC-PBM was *O*-GlcNAcylated by OGT in HEK293T cells (Fig. 1d and Extended Data Fig. 1b), and the modification occurred at Ser1159 and Thr1306 (Extended Data Fig. 1c,d). The *O*-GlcNAcylation levels of wild-type (WT) GFP-SynGAP CC-PBM and its S1159A and T1306A mutants were compared by chemoenzymatic labelling using a mutant galactosyltransferase (Y289L GalT1), which recognizes *O*-GlcNAc and attaches an *N*-azidoacetylgalactosamine (GalNAz) moiety from UDP-*N*-acetylgalactosamine (UDP-GalNAz)[26]. After click reaction with alkyne-biotin and enrichment with streptavidin, immunoblotting showed that *O*-GlcNAcylation of the S1159A and T1306A mutants decreased to ~85% and 30% of WT, indicating T1306 as a major *O*-GlcNAcylation site of SynGAP CC-PBM (Fig. 1e). Because SynGAP-α1 has many additional *O*-GlcNAcylation sites, mutation of T1306 alone did not significantly lower the overall *O*-GlcNAcylation level of the full-length SynGAP-α1 (Supplementary Fig. 1), which underlines the importance of SynGAP CC-PBM for dissecting the function of T1306 *O*-GlcNAc. Importantly, *O*-GlcNAcylation of T1306 was detected by MS on endogenous SynGAP-α1 from the rat brain, indicating the physiological relevance of this modification (Fig. 1f).

Semisynthesis of site-specifically *O*-GlcNAcylated SynGAP CC-PBM. *O*-GlcNAcylation is sub-stoichiometric and often occurs on multiple sites of a modified protein, as in the case of SynGAP. It is therefore challenging to site-specifically elucidate the function of *O*-GlcNAcylation on SynGAP CC-PBM. To overcome this issue, we employed a semisynthesis strategy, expressed protein ligation (EPL)[27,28], to generate two *O*-GlcNAcylated SynGAP CC-PBM proteins—SynGAP CC-PBM-T1306^{OG} (hereafter referred to as SynGAP-T1306^{OG}) and SynGAP CC-PBM-S1159^{OG} (hereafter referred to as SynGAP-S1159^{OG})—which were site-specifically and stoichiometrically *O*-GlcNAcylated at T1306 and S1159, respectively (Fig. 2a). Given that SynGAP CC-PBM has no native Cys, the requisite thiol-containing amino acid at the ligation site, we used thiol-derived Val and Ala, which fulfil EPL and afterwards can be converted back to native Val and Ala via desulfurization chemistry[29,30].

For SynGAP-T1306^{OG}, we envisioned that disconnection between W1302 and V1303 would allow for ligation–desulfurization at γ-thiol Val (V$^{\gamma SH}$1303). The N-terminal fragment of SynGAP CC-PBM (A1150–W1302) fused with an engineered DnaE intein from *Anabaena variabilis* was recombinantly expressed in *Escherichia coli*, and the isolated protein was treated with sodium 2-mercaptoethanesulfonate (MESNa) to generate the requisite C-terminal thioester, as characterized by liquid chromatography (LC)-MS (Supplementary Fig. 2a–e). The C-terminal hexapeptide (V$^{\gamma SH}$1303-T1306^{OG}-V1308) with V1303 substituted with γ-thiol valine and T1306 *O*-GlcNAc-modified was chemically synthesized using solid-phase peptide synthesis (Supplementary Fig. 3a,b). Ligation of the recombinant protein with the synthetic peptide, followed by desulfurization, produced the SynGAP-T1306^{OG} protein with >95% purity (Fig. 2b and Supplementary Fig. 2f–i). Of note, the N-terminal fragment of SynGAP CC-PBM contained four residual amino acids after cleavage of the tags, which remained at the N terminus of SynGAP-T1306^{OG}.

For SynGAP-S1159^{OG}, disconnection between S1165 and A1166 allowed for ligation–desulfurization at C1166. Using peptidyl azide-based EPL[31], the chemically synthesized *O*-GlcNAcylated peptide hydrazide (A1150-S1159^{OG}-S1165-NHNH$_2$; Supplementary Fig. 3c,d) was ligated with the C-terminal protein fragment (C1166–V1308), which was recombinantly expressed with the native A1166 mutated to cysteine (Supplementary Fig. 4a–e). Subsequent desulfurization[30] converted C1166 back to the native alanine residue, giving SynGAP-S1159^{OG} with >95% purity (Fig. 2c and Supplementary Fig. 4f,g).

By using the non-*O*-GlcNAcylated peptides (Supplementary Fig. 3e,f), the non-*O*-GlcNAcylated SynGAP CC-PBM proteins were synthesized via the synthetic routes for SynGAP-T1306^{OG} and SynGAP-S1159^{OG}, respectively (Fig. 2d and Supplementary Fig. 5). The semisynthetic proteins were then refolded by gradient dialysis against urea at decreasing concentrations. Using the recombinantly expressed SynGAP CC-PBM as a comparison, circular dichroism

Fig. 2 | EPL synthesis of site-specifically *O*-GlcNAcylated SynGAP CC-PBM indicates inhibition of LLPS by T1306 *O*-GlcNAcylation. a, Schematic of EPL synthesis of SynGAP-T1306^{OG} and SynGAP-S1159^{OG}. **b**–**d**, Electrospray ionization (ESI)-MS spectra of EPL-synthesized SynGAP-T1306^{OG} (**b**), SynGAP-S1159^{OG} (**c**) and SynGAP CC-PBM (**d**), showing good matches with their calculated molecular weight. The insets show the deconvoluted MS spectra. a.u., arbitrary unit. **e**, CD spectra of SynGAP CC-PBM variants: recombinant (REC) SynGAP CC-PBM, EPL-synthesized SynGAP CC-PBM, SynGAP-T1306^{OG} and SynGAP-S1159^{OG}. Δε, molar absorptivity. **f**, In-gel fluorescence scanning results showing SynGAP CC-PBM, SynGAP-T1306^{OG} and SynGAP-S1159^{OG} incubated with Y298L GalT1 and UDP-GalNAz, and reacted with alkyne-Cy5. CBB-stained gel is shown as the loading control. **g**, Time-lapse fluorescence images showing LLPS of PSD-95 PSG (with 1% conjugated with the TAMRA fluorophore) with recombinant SynGAP CC-PBM, semisynthetic SynGAP CC-PBM, SynGAP-S1159^{OG} or SynGAP-T1306^{OG}. Scale bar, 10 μm. White arrowheads indicate droplet fusion and growth. Yellow arrowheads indicate droplets newly settled on the coverslip. **h**, SDS–PAGE gel showing the distributions of proteins in the supernatant (S) and pellet (P) in the sedimentation-based assay for various SynGAP CC-PBM/PSD-95 PSG mixtures. The bar graph shows quantification of the protein distributions represented as mean ± s.d. Differences were assessed by one-way ANOVA followed by Tukey's multiple comparisons test with 95% CI; $P < 0.05$ is considered significant. In **f**–**h**, representative results are shown from three independent experiments. In **g** and **h**, the concentration of each protein was 80 μM.

(CD) spectroscopy suggested that the semisynthetic proteins SynGAP CC-PBM, SynGAP-T1306^{OG} and SynGAP-S1159^{OG} were correctly folded in the same manner as recombinant SynGAP CC-PBM and that *O*-GlcNAcylation did not noticeably alter the structure of SynGAP CC-PBM (Fig. 2e). In agreement with the MS results (Fig. 2b–d and Supplementary Figs. 2i, 5g and 6e,j), SDS–PAGE analysis showed the semisynthetic proteins at the correct molecular weights (Extended Data Fig. 2). GalT-based chemoenzymatic labelling also confirmed the presence of *O*-GlcNAc on SynGAP-T1306^{OG} and SynGAP-S1159^{OG} (Fig. 2f). Of note, the four residual amino acids at the N terminus rendered SynGAP-T1306^{OG} a slightly higher molecular weight than SynGAP-S1159^{OG}.

SynGAP T1306 *O*-GlcNAc inhibits LLPS by blocking interaction with PSD-95. As a characteristic feature of LLPS, mixing 80 µM recombinant or semisynthetic non-*O*-GlcNAcylated SynGAP CC-PBM with PSD-95 PSG at a 1:1 molar ratio led to sphere-shaped liquid droplets, which gradually fused with each other, as shown

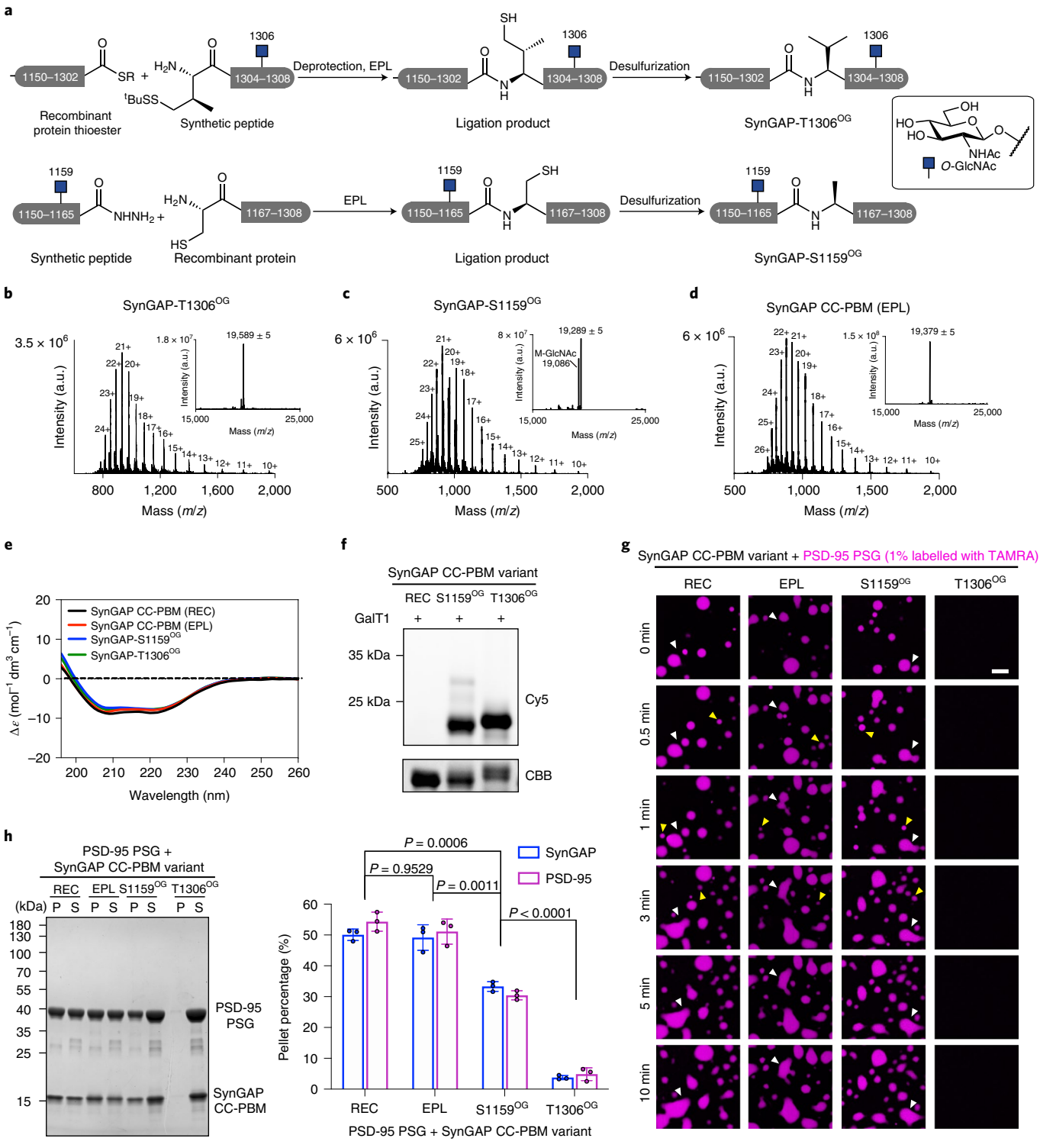

by time-lapse fluorescence microscopy (Fig. 2g). The PSD-95 PSG or SynGAP CC-PBM protein alone could not undergo LLPS (Extended Data Fig. 3a). Strikingly, when SynGAP-T1306^{OG} was mixed with PSD-95 PSG, no liquid droplet was observed. For the mixture of SynGAP-S1159^{OG} and PSD-95 PSG, LLPS with slightly smaller droplets occurred, in a similar manner to the mixture of SynGAP CC-PBM and PSD-95 PSG (Fig. 2g and Extended Data Fig. 3b). Fluorescence recovery after photo-bleaching (FRAP) analysis on a small region within the droplets exhibited rapid recovery of fluorescence following photo-bleaching, indicating dynamic exchange of PSD-95 PSG between the condensate liquid phase and the aqueous solution (Extended Data Fig. 3c–f). By employing the sedimentation assay, in which the condensed droplets (pellet fraction) were separated from the aqueous phase (supernatant fraction), the distribution of the SynGAP CC-PBM and PSD-95 PSG proteins within the two phases was quantified (Fig. 2h and Supplementary Fig. 6). In the mixture of SynGAP-T1306^{OG} and PSD-95 PSG, minimal amounts of proteins were observed in the pellets, indicating that *O*-GlcNAcylation at T1306 of SynGAP CC-PBM almost completely abolished LLPS with PSD-95 PSG. By contrast, S1159 *O*-GlcNAcylation only slightly reduced the proteins in the condensed liquid phase. These results were consistent with the time-lapse imaging experiments. The physiological concentrations of PSD-95 and SynGAP in the synapse were estimated to be in the range of several micromolar to several tens of micromolar[32–34]. In the presence of 2% PEG_{8000} as the crowding reagent, which mimicked the crowded intracellular environment, SynGAP CC-PBM and PSD-95 PSG at a physiological concentration (5 μM) could undergo LLPS, as shown by time-lapse fluorescence microscopy and the sedimentation-based assay (Extended Data Fig. 4). Similarly, SynGAP-T1306^{OG}, when mixed with PSD-95 PSG at the physiological concentration, almost completely abolished LLPS, whereas SynGAP-S1159^{OG} only exhibited slight suppression of LLPS. Taken together, these results indicate that T1306 *O*-GlcNAcylation of SynGAP effectively suppresses LLPS of the SynGAP/PSD-95 complex. Given that S1159 *O*-GlcNAcylation also has a much lower stoichiometry (Fig. 1e), it should have a minimal effect on suppressing LLPS physiologically.

SynGAP CC-PBM forms a trimer, which binds PSD-95 PSG and induces dimerization[25]. The resulting 3:2 SynGAP CC-PBM/PSD-95 PSG complex further oligomerizes and undergoes LLPS, which is driven by the specific and multivalent interactions between the two proteins[2,3]. Because formation of the SynGAP CC-PBM trimer is required for LLPS, we first tested whether T1306 *O*-GlcNAcylation interfered with trimerization of SynGAP CC-PBM. Size-exclusion chromatography coupled with static light scattering (SEC-SLC) was performed to measure the molecular mass of SynGAP CC-PBM, SynGAP-T1306^{OG} and SynGAP-S1159^{OG} in solution. All three proteins exhibited a molecular mass of ~55 kDa, three times the monomer's molecular mass, which indicated that neither T1306 nor S1159 *O*-GlcNAcylation affects trimer formation (Fig. 3a). In the 1:1 mixture of SynGAP CC-PBM and PSD-95 PSG, formation of the pentamer complex exhibited a molecular mass of ~135 kDa (Extended Data Fig. 5a). SynGAP-S1159^{OG} formed the pentamer complex with PSD-95 PSG, in the same manner as SynGAP did (Extended Data Fig. 5b). In sharp contrast, only peaks matching the SynGAP CC-PBM trimer and the PSD-95 PSG monomer were observed for the mixture of SynGAP-T1306^{OG} and PSD-95 PSG, indicating that SynGAP-T1306^{OG} could not form a complex with SynGAP at all (Fig. 3b). The crystal structure of the SynGAP PBM in complex with PSD-95 PDZ3-C (R306-S412), in which the two proteins were fused together with a flexible linker, revealed that hydrogen bonding between PSD-95 H369 and SynGAP T1306 is important for complex formation (Extended Data Fig. 6a)[25]. Based on the reported crystal structure, we modelled the structure of the PSD-95 PDZ3-C/SynGAP PBM-T1306^{OG} complex by using Rosetta homology modelling. *O*-GlcNAcylation at SynGAP T1306 abolished hydrogen bonding between PSD-95 H369 and SynGAP T1306, thus impairing the SynGAP/PSD-95 interaction (Extended Data Fig. 6b). As assayed by isothermal titration calorimetry (ITC)-based titration, the peptide consisting of the 15 SynGAP C-terminal amino acids bound PSD-95 PSG with an affinity of $K_d = 1.15$ μM, and the T1306 *O*-GlcNAcylated peptide could not bind PSD-95 PSG (Fig. 3c and Supplementary Fig. 7). In addition, we mutated T1306 to alanine, which should abolish hydrogen bonding to PSD-95 H369 in a similar manner to *O*-GlcNAcylation. As expected, the SynGAP CC-PBM-T1306A completely inhibited LLPS of SynGAP CC-PBM/PSD-95 PSG (Extended Data Fig. 7). As a control, mutation of S1159 did not affect LLPS. To confirm that disrupting of the interaction between SynGAP and PSD-95 by the T1306 *O*-GlcNAc of SynGAP is responsible for LLPS suppression, we assayed the effects of the 15-amino-acid peptides on pre-formed SynGAP CC-PBM/PSD-95 PSG condensates both in vitro and in living cells. Without the CC domain, the 15-amino-acid peptide is unable to form trimers. Although adding the non-*O*-GlcNAcylated peptide reversed the SynGAP CC-PBM/PSD-95 PSG LLPS and dispersed the condensates into homogeneous solution, T1306 *O*-GlcNAcylation abolished the ability of the peptide to inhibit LLPS (Fig. 3d). GFP-SynGAP CC-PBM and RFP-PSD-95 PSG were co-expressed in HEK293T cells, in which the SynGAP CC-PBM / PSD-95 PSG droplets formed through LLPS were observed and confirmed by FRAP analysis (Extended Data Fig. 8). The naked and *O*-GlcNAcylated SynGAP peptides were delivered to the cytosol of HEK293T cells expressing GFP-SynGAP CC-PBM and RFP-PSD-95 PSG by the micropipette of a patch-clamp system (Supplementary Fig. 8). Time-lapse fluorescence microscopy revealed that the naked but not the T1306 *O*-GlcNAcylated peptide could disperse the condensed liquid droplets in live cells (Fig. 3e). Together, these results demonstrate that T1306 *O*-GlcNAcylation impairs the interaction between SynGAP CC-PBM and PSD-95 PSG, which serves as a mechanism of suppressing LLPS of the complex.

Fig. 3 | SynGAP Thr1306 *O*-GlcNAc disrupts interaction with PSD-95. a, SEC-SLC analysis of SynGAP CC-PBM, SynGAP-S1159^{OG} and SynGAP-T1306^{OG}. The calculated molecular mass and fitting error are shown for each peak. **b**, SEC-SLC analysis of PSD-95 PSG, SynGAP-T1306^{OG} and a 1:1 mixture of PSD-95 PSG and SynGAP-T1306^{OG}. **c**, ITC curve of non-*O*-GlcNAcylated (Pep) or T1306 *O*-GlcNAcylated peptide (OG-Pep) titrated into PSD-95. **d**, Time-lapse DIC images showing addition of Pep or OG-Pep to the pre-formed SynGAP/PSD-95 condensates. The dashed boxes indicate droplets dispersed rapidly and remaining unchanged, respectively. Scale bars, 10 μm. White arrowheads indicate shrinking droplets, and yellow arrowheads droplet growth and fusion. Representative results are shown from three independent experiments. **e**, Left: time-lapse red fluorescent protein (RFP) fluorescence images showing HEK293T cells co-expressing RFP-PSD-95 PSG and GFP-SynGAP CC-PBM, to which vehicle, Pep or OG-Pep was delivered into the cytosol by micropipettes. The white arrowheads indicate the droplets shown in the inserted zoomed images. The colour-coded scales represent the fluorescence intensity. Scale bar, 10 μm. Right: line graph showing statistical analysis of changes of relative fluorescence intensity of the droplets in HEK293T cells during peptide delivery. The fold change was normalized to the fluorescence intensity at the beginning of delivery. Error bars represent mean ± s.d. One droplet was analysed for each cell and for each group, and 15 droplets from at least three independent experiments were analysed. Differences were assessed by one-way ANOVA followed by Tukey's multiple comparisons test (5 min) or Dunnett's multiple comparisons test (10–20 min) with 95% CI; $P < 0.05$ is considered significant.

Dominant-negative effect of SynGAP T1306 *O*-GlcNAc on LLPS. Considering that *O*-GlcNAcylation is substoichiometric in living neurons, we wondered whether and how it could serve as an effective regulator of LLPS. We hypothesized that SynGAP T1306 *O*-GlcNAc could suppress LLPS of SynGAP/PSD-95 in a dominant-negative manner; that is, *O*-GlcNAcylation of SynGAP would function more effectively than removing or degrading an equal portion of the SynGAP protein (Fig. 4a). To test this hypothesis, SynGAP-T1306^{OG} and SynGAP CC-PBM were denatured to monomers and mixed at 1:3 ratio, followed by refolding to produce the overall 25% *O*-GlcNAcylated SynGAP CC-PBM trimer, which consisted of the proteoforms with zero, one, two and three *O*-GlcNAc at a ratio of 42.2:42.2:14.0:1.6 (Extended Data Fig. 9a). Comparing to LLPS of PSD-95 PSG and SynGAP CC-PBM, each at 80 μM, lowering the concentration of SynGAP CC-PBM by 25% to 60 μM resulted in a slight decrease in the formation of liquid droplets (Fig. 4b and

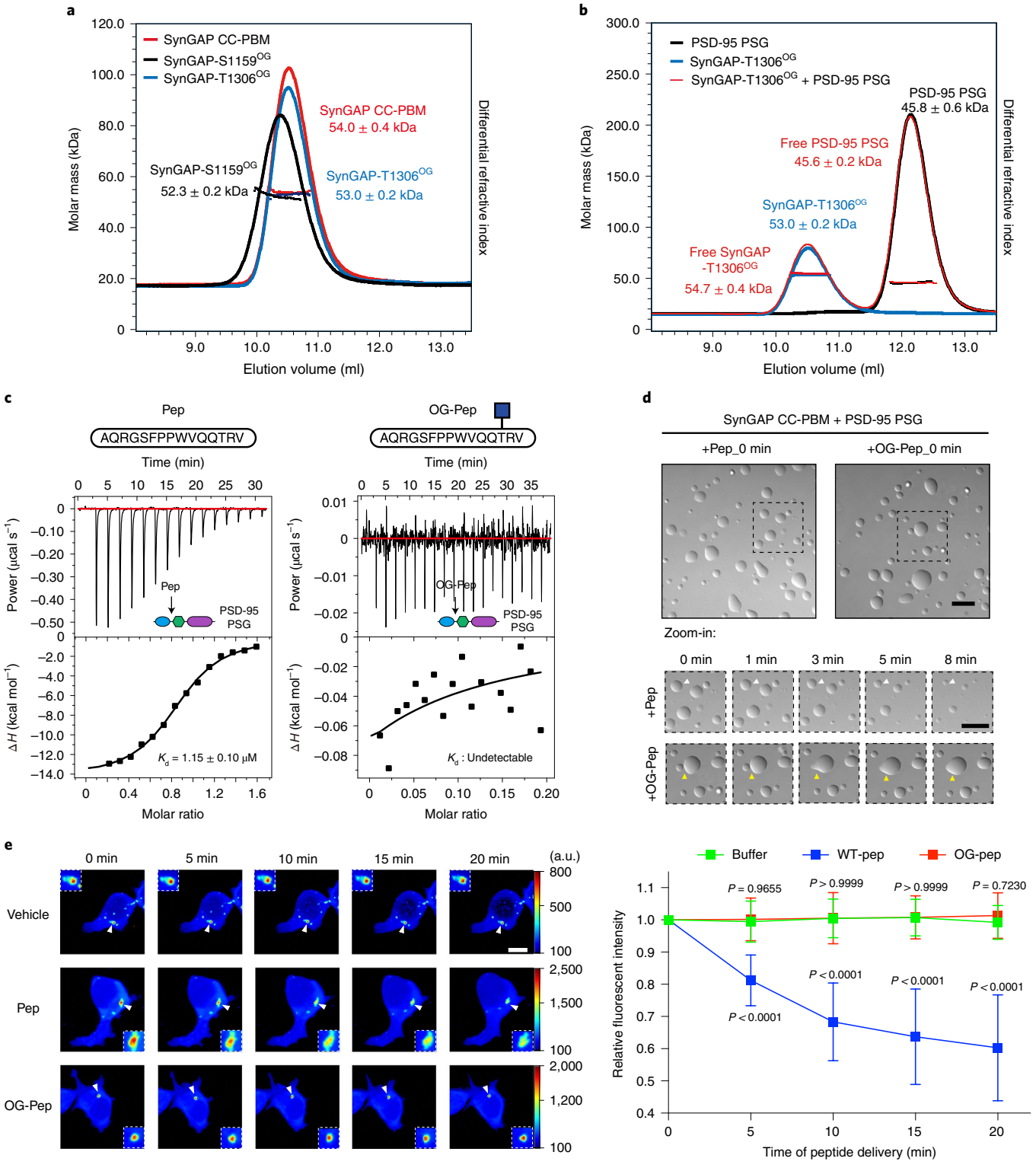

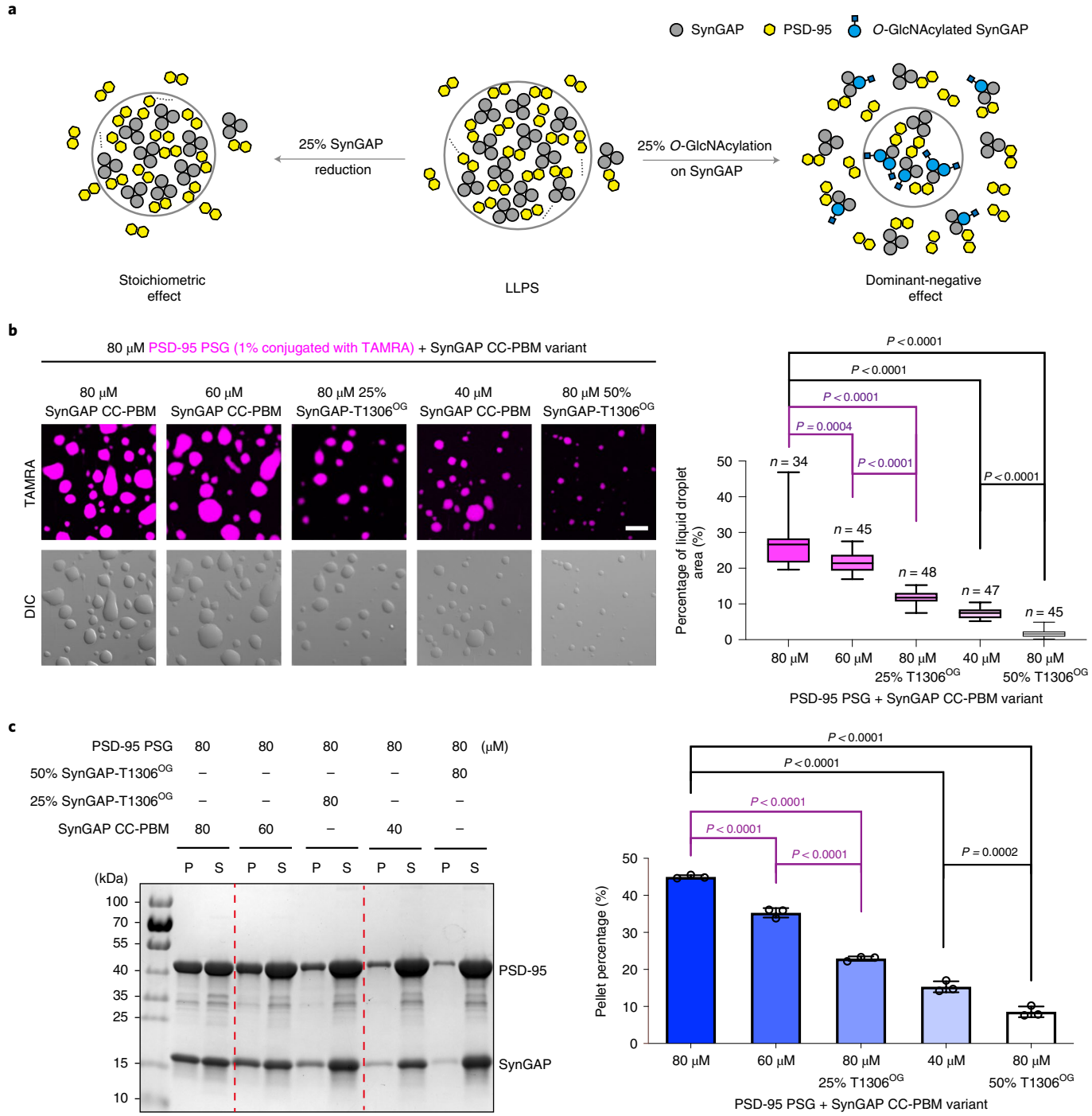

Fig. 4 | *O*-GlcNAc regulates SynGAP/PSD-95 LLPS in a dominant-negative manner. a, Schematic showing the dominant-negative effect of *O*-GlcNAcylation on SynGAP/PSD-95 LLPS. **b**, Fluorescence and DIC images showing LLPS of PSD-95 (with 1% conjugated with TAMRA fluorophore) mixed with SynGAP at the designated concentrations and *O*-GlcNAcylated ratios for 10 min. Scale bar, 10 μm. Box-and-whiskers plot showing statistical analysis of the liquid droplet areas. The horizontal lines mark the maximum, median and minimum values of the data, and boxes mark upper and lower quartiles. For each group, at least 30 fluorescence images from at least three independent experiments were analysed. **c**, SDS–PAGE gel showing the distributions of PSD-95 and SynGAP in the supernatant (S) and pellet (P) in the sedimentation-based assay. The bar graph shows quantification of the distributions. The quantification results are from three independent experiments and are represented as mean ± s.d. Differences were assessed by one-way ANOVA followed by Dunnett's multiple comparisons test (**b**) or Tukey's multiple comparisons test (**c**) with 95% CI; $P < 0.05$ is considered significant.

Extended Data Fig. 9b). When the overall 25% *O*-GlcNAcylated SynGAP CC-PBM at 80 μM was mixed with PSD-95 PSG, a much more dramatic decrease was observed. Similar results were observed with the sedimentation assay (Fig. 4c). Furthermore, the overall 50% *O*-GlcNAcylated SynGAP CC-PBM was similarly prepared, and also showed a lower efficiency in condensed-phase formation than SynGAP CC-PBM at half the amount (Fig. 4b,c). When the overall *O*-GlcNAcylation stoichiometry was increased to 75%, LLPS of

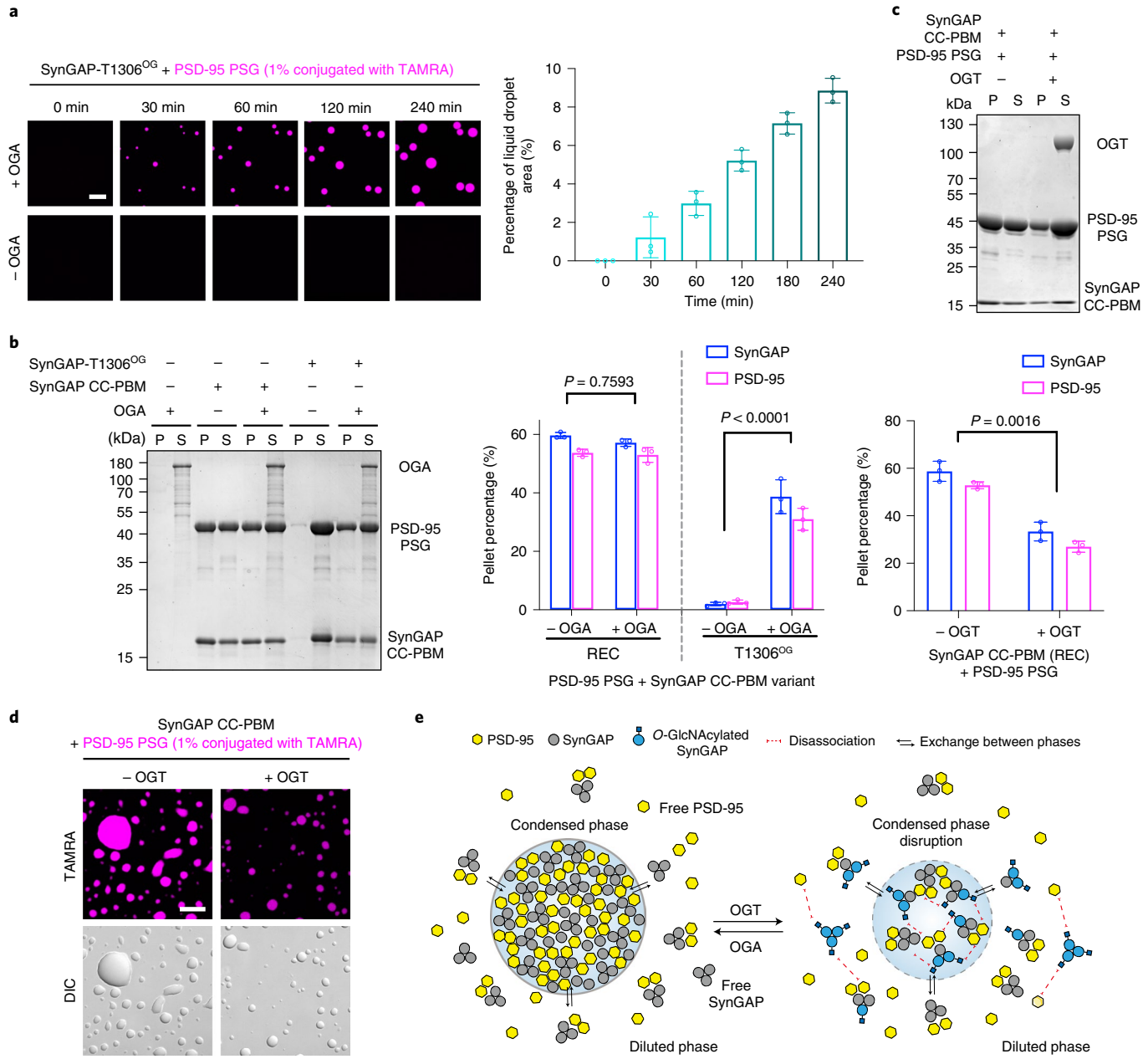

Fig. 5 | The LLPS between SynGAP CC-PBM and PSD-95 PSG could be reversibly regulated by OGT and OGA. a, Representative time-lapse fluorescent images showing LLPS of the mixture of 80 μM PSD-95 PSG and SynGAP-T1306^{OG} in the presence or absence of OGA. The bar graph shows statistical analysis of the liquid droplet areas when OGA was present. **b**, SDS–PAGE gel showing the distributions of PSD-95 and SynGAP after incubation of the mixture of 50 μM PSD-95 PSG and SynGAP CC-PBM or SynGAP-T1306^{OG} with or without OGA for 4 h. Differences were assessed by one-way ANOVA followed by Tukey's multiple comparisons test with 95% CI; $P < 0.05$ is considered significant. **c**, SDS–PAGE gel showing the distributions of PSD-95 and SynGAP after mixing PSD-95 with SynGAP pre-treated with OGT and UDP-GlcNAc or non-*O*-GlcNAcylated SynGAP for 10 min. Unpaired two-tailed Student's *t*-test with 95% CI was used to determine difference; $P < 0.05$ is considered significant. **d**, Representative fluorescence and bright-field images showing LLPS of PSD-95 with SynGAP pre-treated with OGT and UDP-GlcNAc or non-*O*-GlcNAcylated SynGAP for 10 min. For fluorescent images in **a** and **d**, scale bars, 10 μm. In **a**–**c**, the bar graphs show quantification of the distributions. In **a**–**d**, representative results are shown from three independent experiments. **e**, Proposed model of the regulatory role of *O*-GlcNAcylation in SynGAP/PSD-95 LLPS.

PSD-95 PSG/SynGAP CC-PBM was almost completely suppressed (Extended Data Fig. 9c). In addition, the dominant-negative effect of T1306 *O*-GlcNAcylation of SynGAP CC-PBM was observed at various concentrations of PSD-95 PSG/SynGAP CC-PBM, and it appeared that this effect was more apparent at low concentrations (Extended Data Fig. 9d). Taken together, these results demonstrate a dominant-negative effect of SynGAP T1306 *O*-GlcNAcylation in LLPS of PSD-95 PSG/SynGAP CC-PBM.

Regulation of PSD-95/SynGAP LLPS by OGT and OGA. Because OGT and OGA are highly expressed in the brain, with OGT more enriched in the PSD[18,19], we asked whether OGT and OGA could reversibly modulate PSD-95/SynGAP LLPS. We first showed that purified OGA could effectively remove the majority of *O*-GlcNAc from SynGAP-T1306^{OG} (Extended Data Fig. 10a,b). To the mixture of PSD-95 PSG and SynGAP-T1306^{OG}, in which LLPS was suppressed by *O*-GlcNAc, was added purified OGA (Fig. 5a). After 30 min,

liquid droplets started to appear and the droplet size increased gradually. Using the sedimentation assay, we showed that OGA treatment on the mixture of PSG-95 PSG and SynGAP-T1306^{OG} for 4 h resulted in LLPS to an extent close to that for the mixture of PSD-95 PSG and SynGAP CC-PBM (Fig. 5b). To evaluate OGT regulation, the non-*O*-GlcNAcylated SynGAP CC-PBM was incubated with OGT and UDP-GlcNAc, which resulted in *O*-GlcNAcylation of SynGAP CC-PBM with a stoichiometry of ~26% (Extended Data Fig. 10c,d). Both the sedimentation assay and imaging of the liquid droplets showed that OGT treatment markedly impaired LLPS (Fig. 5c,d). Taken together, these results demonstrate that the *O*-GlcNAc-dependent LLPS of PSD-95/SynGAP is reversibly regulated by OGT and OGA (Fig. 5e).

Discussion

EPL-based semisynthesis enables us to obtain the homogeneous *O*-GlcNAcylated SynGAP CC-PBM proteins. By using the simplified PSD-95 PSG/SynGAP CC-PBM condensate, our studies reveal *O*-GlcNAc as a regulator for LLPS of PSD-95/SynGAP. Importantly, we demonstrate that regulation of PSD-95/SynGAP LLPS by *O*-GlcNAcylation is modification site-dependent. Mechanistically, *O*-GlcNAcylation at SynGAP T1306, one of the four amino-acid residues of the PBM of SynGAP, blocks hydrogen bonding between SynGAP T1306 and PSD-95 H369 in the PDZ3 domain, which impairs the interaction between SynGAP and PSD-95 and thus suppresses LLPS of the complex. It should be noted that the LLPS experiments in this work are performed with SynGAP CC-PBM and PSD-95 PSG, rather than the full-length proteins. Although much more challenging, synthesis of full-length SynGAP proteins that are site-specifically *O*-GlcNAcylated will be an interesting future direction. SynGAP contains an IDR that is N-terminal to the CC domain. Multivalent, weak interactions between IDRs represent a common way through which proteins undergo LLPS[2]. It is therefore interesting to speculate that the IDR of SynGAP may contribute to LLPS of SynGAP/PSD-95, and O-GlcNAcylation occurring on the IDR may contribute to LLPS regulation.

Given that the abundance of SynGAP in the PSD is comparable to that of PSD scaffold proteins such as PSD-95[32], LLPS of the SynGAP/PSD-95 complex has been proposed to facilitate the formation of PSD condensates and enrich SynGAP to the PSD[25,35]. In fact, the formed PSD assembly in excitatory synapses consists of many more PSD proteins, as demonstrated by the reconstituted 6× PSD condensates, which were formed by six PSD components: NR2B, SynGAP, PSD-95, GKAP, Shank and Homer[35]. SynGAP was shown to be selectively enriched in the 6× PSD condensates, further supporting that LLPS enriches SynGAP to the PSD. In line with this hypothesis, enrichment of SynGAP in dendritic spines was observed in living neurons[23,24,36]. The PBM (that is, the last four residues, QTRV^{1308}) is specific for the α1 isoform of SynGAP and is essential for PSD-95 binding and synaptic plasticity[37]. Point mutations or deletion of the whole PBM abolish SynGAP binding to PSD-95, which decreases SynGAP enrichment in the PSD[25,38,39]. Because T1306 *O*-GlcNAc affects the binding between SynGAP and PSD-95 in a similar manner, we postulate that *O*-GlcNAcylation at SynGAP T1306 may inhibit PSD condensate formation in neurons by impairing PSD-95/SynGAP LLPS.

On the other hand, SynGAP not only serves as one of the components of PSD condensates, but also possesses GAP enzymatic activity and functions as a synaptic activity 'brake' in excitatory synapses[22]. Long-term potentiation (LTP) induction rapidly disperses SynGAP from the PSD, which promotes synapse activation and spine enlargement[36]. Similarly, point mutations and deletion of PBM lead to pre-maturation and enlargement of spines[25,38], increased synaptic strength[39] and stronger synaptic plasticity[25]. In this part of regulation, we hypothesize that T1306 *O*-GlcNAcylation of SynGAP disperses it from the PSD condensates in excitatory synapses, which favours synapse enlargement and activation. In support of this hypothesis, knockout of OGT in excitatory neurons leads to fewer morphologically mature synapses[19].

In the presynaptic compartment, the active zone and the reserve synaptic vesicle pool also involve LLPS-mediated condensates[40,41]. It will be interesting to investigate whether *O*-GlcNAc regulates these LLPS processes in neurons. More broadly, it is appealing to hypothesize that the ubiquitous *O*-GlcNAcylation may serve as a generic regulator of various LLPS processes, including LLPS of RNA-binding proteins[6]. In support of this hypothesis, the FG domains of nucleoporins can form hydrogels and *O*-GlcNAc modification on nucleoporins has been shown to increase hydrogel permeability[42]. Furthermore, the coat nucleoporin complex was found to generate a separate solution phase[43]. Similarly, *O*-GlcNAc has been implicated in regulating aggregation of proteins, such as tau[44] and α-synuclein[45], and the aggregation of these proteins may involve LLPS[14,46].

Of note, *O*-GlcNAcylation may also promote protein–protein interactions[47–49]. Whether *O*-GlcNAc can have a promoting effect on LLPS therefore remains an open question. Finally, SynGAP is also phosphorylated at multiple sites, some of which play important roles in regulating GAP activity and PSD enrichment[36,50]. The semisynthetic approach is also well suited to studying the regulatory roles of phosphorylation in LLPS of SynGAP/PSD-95 and the possible crosstalk between phosphorylation and *O*-GlcNAcylation in LLPS regulation.

Online content

Any methods, additional references, Nature Research reporting summaries, source data, extended data, supplementary information, acknowledgements, peer review information; details of author contributions and competing interests; and statements of data and code availability are available at https://doi.org/10.1038/s41557-022-00946-9.

Received: 18 June 2020; Accepted: 7 April 2022;
Published online: 30 May 2022

References

1. Shin, Y. & Brangwynne, C. P. Liquid phase condensation in cell physiology and disease. *Science* **357**, eaaf4382 (2017).
2. Banani, S. F., Lee, H. O., Hyman, A. A. & Rosen, M. K. Biomolecular condensates: organizers of cellular biochemistry. *Nat. Rev. Mol. Cell Biol.* **18**, 285–298 (2017).
3. Chen, X., Wu, X., Wu, H. & Zhang, M. Phase separation at the synapse. *Nat. Neurosci.* **23**, 301–310 (2020).
4. Shin, Y. et al. Liquid nuclear condensates mechanically sense and restructure the genome. *Cell* **175**, 1481–1491 (2018).
5. Hondele, M. et al. DEAD-box ATPases are global regulators of phase-separated organelles. *Nature* **573**, 144–148 (2019).
6. Hofweber, M. & Dormann, D. Friend or foe—post-translational modifications as regulators of phase separation and RNP granule dynamics. *J. Biol. Chem.* **294**, 7137–7150 (2019).
7. Nott, T. J. et al. Phase transition of a disordered nuage protein generates environmentally responsive membraneless organelles. *Mol. Cell* **57**, 936–947 (2015).
8. Qamar, S. et al. FUS phase separation is modulated by a molecular chaperone and methylation of arginine cation-π interactions. *Cell* **173**, 720–734 (2018).
9. Hofweber, M. et al. Phase separation of FUS is suppressed by its nuclear import receptor and arginine methylation. *Cell* **173**, 706–719 (2018).
10. Ryan, V. H. et al. Mechanistic view of hnRNPA2 low-complexity domain structure, interactions, and phase separation altered by mutation and arginine methylation. *Mol. Cell* **69**, 465–479 (2018).
11. Tsang, B. et al. Phosphoregulated FMRP phase separation models activity-dependent translation through bidirectional control of mRNA granule formation. *Proc. Natl. Acad. Sci. USA* **116**, 4218–4227 (2019).
12. Murray, D. T. et al. Structure of FUS protein fibrils and its relevance to self-assembly and phase separation of low-complexity domains. *Cell* **171**, 615–627 (2017).
13. Wang, A. et al. A single N-terminal phosphomimic disrupts TDP-43 polymerization, phase separation and RNA splicing. *EMBO J.* **37**, e97452 (2018).

14. Ambadipudi, S., Biernat, J., Riedel, D., Mandelkow, E. & Zweckstetter, M. Liquid–liquid phase separation of the microtubule-binding repeats of the Alzheimer-related protein Tau. *Nat. Commun.* **8**, 275 (2017).
15. Kim, T. H. et al. Phospho-dependent phase separation of FMRP and CAPRIN1 recapitulates regulation of translation and deadenylation. *Science* **365**, 825–829 (2019).
16. Guo, Y. E. et al. Pol II phosphorylation regulates a switch between transcriptional and splicing condensates. *Nature* **572**, 543–548 (2019).
17. Yang, X. & Qian, K. Protein *O*-GlcNAcylation: emerging mechanisms and functions. *Nat. Rev. Mol. Cell Biol.* **18**, 452–465 (2017).
18. Lagerlof, O. & Hart, G. W. *O*-GlcNAcylation of neuronal proteins: roles in neuronal functions and in neurodegeneration. *Adv. Neurobiol.* **9**, 343–366 (2014).
19. Lagerlöf, O., Hart, G. W. & Huganir, R. L. O-GlcNAc transferase regulates excitatory synapse maturity. *Proc. Natl. Acad. Sci. USA* **114**, 1684–1689 (2017).
20. Trinidad, J. C. et al. Global identification and characterization of both O-GlcNAcylation and phosphorylation at the murine synapse. *Mol. Cell Proteomics* **11**, 215–229 (2012).
21. Li, W. et al. Characterization of a novel SynGAP isoform, SynGAP-β. *J. Biol. Chem.* **276**, 21417–21424 (2001).
22. Gamache, T. R., Araki, Y. & Huganir, R. L. Twenty years of SynGAP research: from synapses to cognition. *J. Neurosci.* **40**, 1596–1605 (2020).
23. Chen, H.-J., Rojas-Soto, M., Oguni, A. & Kennedy, M. B. A synaptic Ras-GTPase Activating Protein (p135 SynGAP) inhibited by CaM Kinase II. *Neuron* **20**, 895–904 (1998).
24. Kim, J. H., Liao, D., Lau, L.-F. & Huganir, R. L. SynGAP: a synaptic RasGAP that associates with the PSD-95/SAP90 protein family. *Neuron* **20**, 683–691 (1998).
25. Zeng, M. et al. Phase transition in postsynaptic densities underlies formation of synaptic complexes and synaptic plasticity. *Cell* **166**, 1163–1175(2016).
26. Clark, P. M. et al. Direct in-gel fluorescence detection and cellular imaging of O-GlcNAc-modified proteins. *J. Am. Chem. Soc.* **130**, 11576–11577 (2008).
27. Muir, T. W., Sondhi, D. & Cole, P. A. Expressed protein ligation: a general method for protein engineering. *Proc. Natl. Acad. Sci. USA* **95**, 6705–6710 (1998).
28. Shah, N. H., Dann, G. P., Vila-Perelló, M., Liu, Z. & Muir, T. W. Ultrafast protein splicing is common among cyanobacterial split inteins: implications for protein engineering. *J. Am. Chem. Soc.* **134**, 11338–11341 (2012).
29. Chen, J., Wan, Q., Yuan, Y., Zhu, J. & Danishefsky, S. J. Native chemical ligation at valine: a contribution to peptide and glycopeptide synthesis. *Angew. Chem. Int. Ed.* **47**, 8521–8524 (2008).
30. Wan, Q. & Danishefsky, S. J. Free-radical-based, specific desulfurization of cysteine: a powerful advance in the synthesis of polypeptides and glycopolypeptides. *Angew. Chem. Int. Ed.* **46**, 9248–9252 (2007).
31. Fang, G. et al. Protein chemical synthesis by ligation of peptide hydrazides. *Angew. Chem. Int. Ed.* **50**, 7645–7649 (2011).
32. Cheng, D. et al. Relative and absolute quantification of postsynaptic density proteome isolated from rat forebrain and cerebellum. *Mol. Cell Proteomics* **5**, 1158–1170 (2006).
33. Sugiyama, Y., Kawabata, I., Sobue, K. & Okabe, S. Determination of absolute protein numbers in single synapses by a GFP-based calibration technique. *Nat. Methods* **2**, 677–684 (2005).
34. Zeng, M. et al. Phase separation-mediated TARP/MAGUK complex condensation and AMPA receptor synaptic transmission. *Neuron* **104**, 529–543 (2019).
35. Zeng, M. et al. Reconstituted postsynaptic density as a molecular platform for understanding synapse formation and plasticity. *Cell* **174**, 1172–1187 (2018).
36. Araki, Y., Zeng, M., Zhang, M. & Huganir, R. L. Rapid dispersion of SynGAP from synaptic spines triggers AMPA receptor insertion and spine enlargement during LTP. *Neuron* **85**, 173–189 (2015).
37. Araki, Y. et al. SynGAP isoforms differentially regulate synaptic plasticity and dendritic development. *eLife* **9**, e56273 (2020).
38. Vazquez, L. E., Chen, H.-J., Sokolova, I., Knuesel, I. & Kennedy, M. B. SynGAP regulates spine formation. *J. Neurosci.* **24**, 8862–8872 (2004).
39. Rumbaugh, G., Adams, J. P., Kim, J. H. & Huganir, R. L. SynGAP regulates synaptic strength and mitogen-activated protein kinases in cultured neurons. *Proc. Natl. Acad. Sci. USA* **103**, 4344–4351 (2006).
40. Wu, X. et al. RIM and RIM-BP form presynaptic active-zone-like condensates via phase separation. *Mol. Cell* **73**, 971–984.e5 (2019).
41. Milovanovic, D., Wu, Y., Bian, X. & Camilli, P. D. A liquid phase of synapsin and lipid vesicles. *Science* **361**, eaat5671 (2018).
42. Labokha, A. A. et al. Systematic analysis of barrier-forming FG hydrogels from *Xenopus* nuclear pore complexes. *EMBO J.* **32**, 204–218 (2013).
43. Lin, D. H. et al. Architecture of the symmetric core of the nuclear pore. *Science* **352**, aaf1015 (2016).
44. Yuzwa, S. A. et al. Increasing *O*-GlcNAc slows neurodegeneration and stabilizes tau against aggregation. *Nat. Chem. Biol.* **8**, 393–399 (2012).
45. Marotta, N. P. et al. *O*-GlcNAc modification blocks the aggregation and toxicity of the protein α-synuclein associated with Parkinson's disease. *Nat. Chem.* **7**, 913–920 (2015).
46. Ray, S. et al. Synuclein aggregation nucleates through liquid–liquid phase separation. *Nat. Chem.* **12**, 705–716 (2020).
47. Tarbet, H. J., Toleman, C. A. & Boyce, M. A sweet embrace: control of protein-protein interactions by *O*-linked β-*N*-acetylglucosamine. *Biochemistry* **57**, 13–21 (2017).
48. Qin, W. et al. Quantitative time-resolved chemoproteomics reveals that stable *O*-GlcNAc regulates box C/D snoRNP biogenesis. *Proc. Natl. Acad. Sci. USA* **114**, E6749–E6758 (2017).
49. Hao, Y. et al. Next-generation unnatural monosaccharides reveal that ESRRB O-GlcNAcylation regulates pluripotency of mouse embryonic stem cells. *Nat. Commun.* **10**, 4065 (2019).
50. Walkup, W. G. et al. Phosphorylation of synaptic GTPase-Activating Protein (synGAP) by Ca^{2+}/calmodulin-dependent protein kinase II (CaMKII) and cyclin-dependent kinase 5 (CDK5) alters the ratio of its GAP activity toward Ras and Rap GTPases. *J. Biol. Chem.* **290**, 4908–4927 (2015).

Methods

Cloning. The pEGFP-C2-GFP-SynGAP-α1 res#5, pEGFP-C3-SynGAP CC-PBM, RFP-PSD-95 PSG (the vector was modified based on pEGFP-C3), pET28a-GB1-His_6-SynGAP CC-PBM and pET28a-His_6-PSD-95 PSG plasmids have been described previously[25]. Human ncOGT cDNA was PCR-amplified from the pEGFP-N1-OGT plasmid[49] and cloned into the p3×FLAG-CMV-10 vector for mammalian expression. The pET28a-OGT construct and pET28a-OGA (human full-length OGA) plasmids were gifts from the Peng Wang laboratory at NanKai University. The GFP-SynGAP-α1-T1306A, GFP-SynGAP CC-PBM S1159A and T1306A mutants were generated by PCR-based site-directed mutagenesis. The cDNA encoding the N-terminal fragment of SynGAP CC-PBM (A1150–W1302) was PCR-amplified from the pET28a-GB1-His_6-SynGAP CC-PBM plasmid and cloned into the pET.MG.3C vector. The AvaDnaE-CBD fragment was amplified from the PTXB1 plasmid containing the AvaDnaE N137A intein (a gift from the Xiang Li laboratory at University of Hong Kong) and cloned into the pET.MG.3C-GB1-His_6-SynGAP (A1150–W1302) plasmid to generate pET.MG.3C-GB1-His_6-SynGAP (A1150–W1302)-AvaDNaE-CBD. The C-terminal fragment of SynGAP CC-PBM (C1166–V1308, where AA1166 was mutated from the natural alanine to cysteine) was PCR-amplified from the pET.MG.3C-GB1-His_6-SynGAP CC-PBM plasmid and cloned into the pET28a-SUMO vector (a gift from the Lei Liu laboratory at Tsinghua University) to generate pET28a-His_6-SUMO-SynGAP (C1166–V1308) plasmid. All plasmids were verified by DNA sequencing.

Cell culture and transfection. HEK293T cells (ATCC CRL-11268) were cultured in Dulbecco's modified Eagle medium (DMEM; Gibco) supplemented with 10% fetal bovine serum (FBS; Gibco), 100 U ml^{-1} penicillin and 100 mg ml^{-1} streptomycin (Gibco) at 37 °C and 5% CO_2. Cells in all experiments were within 20 passages and free of mycoplasma contamination. Transfection was performed using VigoFect (Vigorous Biotechnology) for immunoprecipitation experiments or X-tremeGENE (Roche) for imaging experiments, by following the manufacturers' instructions. In VigoFect transfection, the cells were cultured to ~70–80% confluency in 6-cm dishes, followed by transfection with 4–6 μg of plasmid. The cells were changed with fresh DMEM after 12 h and incubated for 48 h before further experiments. In X-tremeGENE transfection, the cells were cultured to ~50% confluency in 35-mm glass-bottom dishes coated with poly-D-lysine, followed by transfection with 0.2–0.6 μg of plasmid. The cells were changed with fresh DMEM after 6 h and incubated for 14 h before further experiments.

Purification of endogenous SynGAP from the rat brain. Wild-type Sprague–Dawley male rats were purchased from the Charles River Laboratory Animal Center, and maintained under specific pathogen-free (SPF) conditions with free access to food and water. All animal experiments were performed in accordance with the guidelines approved by the Institutional Animal Care and Use Committee of Peking University accredited by AAALAC International. The homogenized rat brain tissues were washed with ice-cold phosphate buffered saline (PBS) and lysed in RIPA lysis buffer (50 mM triethanolamine, pH 7.5, 150 mM NaCl, 0.1% SDS, 1% sodium deoxycholate, 0.5% Nonidet P-40 and Complete EDTA-free protease inhibitors (Roche)). The lysate was incubated at 4 °C for 10 min, sonicated and centrifuged at 18,407*g* for 10 min. The supernatant was collected and the precipitate was further lysed with 2% SDS lysis buffer (50 mM Tris-HCl, pH 7.5, 2% SDS, 1 mM EDTA) to adequately release the SynGAP protein, followed by centrifugation at 18,000*g* for 10 min. The two supernatants were combined, diluted with NP-40 lysis buffer (50 mM Tris-HCl, pH 7.5, 150 mM NaCl, 1% Nonidet P-40, 1 mM EDTA), followed by incubation with anti-SynGAP immunoglobulin-G (IgG)-conjugated beads for 4 h at 4 °C. The anti-SynGAP IgG-conjugated beads were prepared by incubation of anti-SynGAP antibody with protein A-agarose beads (NEB). The beads were then washed with cold immunoprecipitation wash buffer (50 mM Tris-HCl, pH 7.5, 400 mM NaCl, 1% Nonidet P-40) four times, and the protein was eluted by boiling the beads with SDS–PAGE loading buffer.

Purification of GFP-SynGAP from HEK293T cells. The HEK293T cells transiently expressing GFP-SynGAP-α1, GFP-SynGAP-α1-S1159A, GFP-SynGAP-α1-T1306A or GFP-SynGAP CC-PBM were lysed and immunoprecipitated with anti-GFP mAb-conjugated magnetic beads (MBL) following the same procedures as described in the previous section.

SDS–PAGE and immunoblotting. For SDS–PAGE analysis, proteins were boiled for 10 min in SDS–PAGE loading buffer and separated with 10% or 12.5% home-made SDS–PAGE gels or 4–20% Mini-PROTEAN TGX Precast Gels (Bio-Rad). For immunoblotting, proteins were separated with SDS–PAGE gels and then transferred onto polyvinylidene fluoride (PVDF) membranes (Immobilon-P, Millipore). The membranes were blocked in TBST buffer (0.05% Tween-20, 150 mM NaCl, 50 mM Tris-HCl, pH 8.0) containing 5% (wt/vol) non-fat milk for 1–4 h at room temperature (r.t.) and incubated with the primary antibodies in the TBST buffer. After washing three times with TBST buffer for 5 min, the membranes were incubated with species-matched horseradish peroxidase (HRP)-conjugated secondary antibodies for 1–2 h at r.t., followed by three washes with TBST buffer. After reaction with ECL Clarify substrates (Bio-Rad), the membranes were visualized by ChemiDoc XRS+ (Bio-Rad) or Tanon-5200Multi (Tanon). When stripping was needed, the membranes were incubated with stripping buffer (CWBIO) at r.t. for 15 min and washed three times in TBST buffer for 5 min. Primary antibodies included anti-SynGAP (Rb, Abcam, ab3344, 1:1,000), anti-GFP (Rb, Abcam, ab32146, 1:10,000), anti-FLAG (Ms, BioLegend, 637301, 1:5,000), anti-O-GlcNAc CTD110.6 (Ms, Santa Cruz, sc-59623, 1:200) and anti-GAPDH-HRP (Ms, Abcam, ab9482, 1:5000). Secondary antibodies included goat anti-mouse IgG H&L HRP (Abcam, ab6789, 1:5,000), goat anti-rabbit IgG H&L HRP (Abcam, ab6721, 1:5,000) and goat anti-mouse IgM HRP (Invitrogen, 31440, 1:5,000). SDS–PAGE and immunoblotting data were processed by ImageLab (version 5.2.1) and ImageJ/Fiji (version 1.5.2a).

Identification of SynGAP *O*-GlcNAcylation sites. The recombinant GFP-SynGAP-α1 and GFP-SynGAP CC-PBM and endogenous SynGAP from the rat brain were resolved on SDS–PAGE gels and stained with Coomassie brilliant blue (CBB). The protein bands were excised, washed with Milli-Q water, and destained twice with destaining buffer (50 mM ammonium bicarbonate and acetonitrile mixed at a 1:1 volume ratio) for 30 min, followed by dehydrating in acetonitrile and rehydrating with 10 mM dithiothreitol (DTT) in 50 mM ammonium bicarbonate solution for 45 min at 56 °C. The gel slices were then treated with 55 mM iodoacetamide in 50 mM ammonium bicarbonate solution for 45 min at r.t. in the dark, followed by dehydrating with acetonitrile. The gel slices were then digested with chymotrypsin (2 ng μl^{-1}) or trypsin (5 ng μl^{-1}) in 50 mM ammonium bicarbonate solution for 12–16 h at 37 °C. The resulting peptides were eluted twice with 200 μl of 50% acetonitrile aqueous solution containing 5% formic acid (vol/vol) and the solvent was evaporated in a vacuum centrifuge.

For GFP-SynGAP-α1 and GFP-SynGAP CC-PBM, the peptides were analysed by an LTQ Velos Pro-Orbitrap Elite mass spectrometer equipped with an EASY-nLC 1000 system (Thermo Fisher Scientific) using the electron-transfer dissociation (ETD) fragmentation mode. For the endogenous SynGAP, the peptides were analysed on a Q-Exactive plus Orbitrap mass spectrometer coupled with an EASY-nLC 1200 system (Thermo Fisher Scientific) using the higher-energy collisional dissociation (HCD) fragmentation mode. MS/MS fragmentation was performed in a data-dependent mode. The ions matching the targeted *m*/*z* values of the predicted *O*-GlcNAcylated SynGAP C-terminal peptides were selected for MS/MS analysis at a resolution of 17,500. The MS/MS data were analysed using Mascot software.

Chemoenzymatic labelling of *O*-GlcNAc on SynGAP proteins. The procedures of chemoenzymatic labelling using Y289L GalT1 and UDP-GalNAz have been described previously[49]. In this work, 75 μl of Y289L GalT1 (2 mg ml^{-1}) and 100 μl of UDP-GalNAz (0.5 mM) were used to label 2 mg of the whole protein lysates, which were precipitated from HEK293T cells expressing GFP-SynGAP CC-PBM, GFP-SynGAP CC-PBM S1159A or GFP-SynGAP CC-PBM T1306A, and the total volume for chemoenzymatic reaction was 2 ml. To quantify the *O*-GlcNAcylation level, the resulting mixtures were click-labelled with biotin (click-labelling conditions: 1 mg ml^{-1} protein, 400 μM pre-mixed $CuSO_4$–BTTAA complex (molar ratio of 1:2 for $CuSO_4$:BTTAA), 100 μM alkyne-PEG_4-biotin and 2.5 mM freshly prepared sodium ascorbate). The proteins were then immunoprecipitated with streptavidin-agarose beads (Thermo Fisher Scientific), eluted by boiling in SDS–PAGE loading buffer and subjected to immunoblot analysis with an anti-GFP antibody (Abcam, ab32146, 1:10,000).

For labelling pure proteins including SynGAP-$T1306^{OG}$, SynGAP-$S1159^{OG}$, SynGAP CC-PBM and OGA- or OGT-treated proteins, 0.2 mg of each protein was chemoenzymatically labelled using the same conditions as above. The resulting proteins were click-labelled with 100 μM alkyne-Cy5 or 2 mM alkyne-PEG_{2k} (J&K Scientific) and resolved on 4–20% SDS–PAGE gels. The Cy5-labelled samples were imaged by Typhoon FLA 9500 (GE Healthcare). The PEGylated samples were stained with CBB to resolve the *O*-GlcNAcylated proteins by mass shift.

Protein expression and purification in *E. coli*. GB1-His_6-SynGAP CC-PBM, GB1-His_6-$SynGAP_{A1150\text{-}W1302}$-AvaDnaE-CBD (protein **1**), His_6-SUMO-$SynGAP_{C1166\text{-}V1308}$ (protein **7**), His_6-PSD-95 PSG, His_6-OGT and His_6-OGA were expressed and purified from *E. coli* BL21 (DE3). Briefly, *E. coli* cells transformed with the plasmids were plated on lysogeny broth (LB) agar plates containing specific antibiotics at 37 °C overnight. Single clones were selected and cultured in liquid LB medium containing specific antibiotics at 37 °C with shaking at 220 r.p.m. overnight. After 1:100 dilution in LB medium containing antibiotics, the culture was grown at 37 °C to an optical density at 600 nm (OD_{600}) of 0.6–0.8 (to an OD_{600} of 1.0 for His_6-OGT and His_6-OGA expression as exceptions). The culture was cooled to 16 °C and induced with isopropyl β-D-1-thiogalactopyranoside (IPTG) at 16 °C for 16–18 h (IPTG induction performed at 37 °C for 4 h for His_6-SUMO-$SynGAP_{C1166\text{-}V1308}$ expression as an exception). The cells were pelleted, resuspended in binding buffer (50 mM Tris-HCl pH 7.8, 500 mM NaCl, 6 mM imidazole, 1 mM phenylmethylsulfonyl fluoride (PMSF)) and lysed. The lysates were centrifuged at 15,000*g* to remove the pellet. The supernatant was then purified using a nickel-charged HisTrap HP column (GE Healthcare) and further purified by size-exclusion chromatography with a column buffer containing 50 mM Tris-HCl pH 7.8, 150 mM NaCl (500 mM NaCl for GB1-His_6-$SynGAP_{A1150\text{-}W1302}$-AvaDnaE-CBD

purification as an exception), 1 mM EDTA and 5 mM DTT (5 mM tris(2-carboxyethyl)phosphine (TCEP) instead for GB1-His_6-SynGAP$_{A1150\text{-}W1302}$-AvaDnaE-CBD purification as an exception). When needed, the N-terminal tags were cleaved by HRV 3C protease (Thermo Fisher Scientific) or Ulp1 (SUMO protease) and separated by another step of size-exclusion chromatography.

EPL synthesis of SynGAP-T1306^{OG}, SynGAP-S1159^{OG} and SynGAP CC-PBM. In procedure A, recombinant GB1-His_6-SynGAP$_{A1150\text{-}W1302}$-AvaDnaE-CBD (protein **1**) was cleaved by HRV 3C protease at r.t. for 12 h. The resulting mixture was first purified by gel filtration on a Superdex 200 column (GE Healthcare), followed by a second purification step using preparative HPLC (20–60% solvent B gradient over 30 min, Proto-300 C4 column). The resulting SynGAP$_{A1150\text{-}W1302}$-AvaDnaE-CBD (protein **2**) was analysed by LC-MS (Waters SQD). After lyophilization, the purified protein **2** (2 mg) was treated with 500 mM MESNa in 2.5 ml of MESNa buffer (50 mM HEPES pH 7.5, 250 mM NaCl, 500 mM MESNa) at 37 °C for 24 h, with gentle stirring. The reaction was monitored by LC-MS. On completion, the thiolysis reaction mixture was purified by preparative HPLC (20–60% solvent B gradient over 30 min, Proto-300 C4 column) to afford protein thioester **3** (0.8 mg, calculated yield, ~84%), which was characterized by LC-MS and lyophilized. The protein thioester **3** (2.0 mg, 1 equiv.) was then reacted with peptide **4** (1.1 mg, 10 equiv.) in 350 µl of ligation buffer I (6 M Gn·HCl, 200 mM NaH_2PO_4, 50 mM TCEP·HCl, 200 mM 4-mercaptophenylacetic acid (MPAA), pH 7.0) under an argon atmosphere at 37 °C for 24 h. The reaction was quenched by addition of a mixture of CH_3CN/H_2O/AcOH (47.5:47.5:5, vol/vol/vol), and further purified by preparative HPLC (10 to 50% solvent B over 30 min, Proto-300 C4 column) to yield ligation product SynGAP$_{A1150\text{-}V1308}$-T1306^{OG}(1303V$^{\gamma SH}$) (protein **5**, 1.8 mg, 87% yield). Under the same conditions, protein thioester **3** (4.8 mg, 1 equiv.) was reacted with peptide **12** (2.2 mg, 10 equiv.) to afford SynGAP$_{A1150\text{-}V1308}$ (1303V$^{\gamma SH}$) (protein **13**, 4.2 mg, 85% yield). Products **5** and **13** were analysed by LC-MS. To convert 1303V$^{\gamma SH}$ to valine, 2 mg of protein **5** or **13** was dissolved in 200 µl of desulfurization buffer (6 M Gn·HCl, 200 mM NaH_2PO_4, pH 7.0) under an argon atmosphere, to which 200 µl of 0.5 M bond-breaker TCEP solution (Pierce), 20 µl of 2-methyl-2-propanethiol and 100 µl of radical initiator (0.1 M VA-044 in water) were added. The reaction mixture was gently stirred at 37 °C for 48 h. On completion, the reaction was diluted with 1 ml of CH_3CN/H_2O/AcOH (47.5:47.5:5, vol/vol/vol) and further purified by preparative HPLC (32 to 36% solvent B over 30 min, Proto-300 C4 column) to yield SynGAP-T1306^{OG} (protein **6**, 1.2 mg, 60% yield) or SynGAP CC-PBM (EPL-C, protein **14**, 1.5 mg, 75% yield). The resulting proteins **6** and **14** were analysed by LC-MS.

In procedure B, recombinant His_6-SUMO-SynGAP$_{C1166\text{-}V1308}$ (protein **7**) was incubated with SUMO protease Ulp1 at r.t. for 4 h, followed by purification by gel filtration on a Superdex 200 column (GE Healthcare) and preparative HPLC (20–60% solvent B gradient over 30 min, Proto-300 C4 column) to afford protein **8**, which was analysed by LC-MS and lyophilized. For peptide ligation, peptide **9** (2.2 mg, 5 equiv.) was dissolved in 220 µl of ligation buffer II (6 M Gn·HCl, 200 mM NaH_2PO_4, pH 3.0–3.1) in a 4-ml sample vial, and sonicated to complete dissolvation. After centrifugation at 3,260*g* for 3 min at r.t., the reaction mixture was placed in a −15 °C ice/salt bath, and gently agitated by magnetic stirring for 15 min, followed by addition of 35 equiv. of 0.2 M $NaNO_2$ aqueous solution to oxidize peptide hydrazine to the corresponding hydrazide. After oxidization for 15 min, 100 equiv. MPAA dissolved in 560 µl of ligation buffer III (6 M Gn·HCl, 200 mM NaH_2PO_4, 200 mM MPAA, pH 7.0) containing 1 equiv. of protein **8** (3.9 mg) was added. The reaction was immediately removed from the ice/salt bath and allowed to warm to r.t., and stirred for 15 min to complete the conversion. To the reaction was slowly added 2 M NaOH solution to pH 6.8–7.0 to initiate the native chemical ligation. The reaction mixture was stirred at 37 °C for 24 h, during which the reaction was monitored by LC-MS. On completion, the reaction was quenched by the addition of an equal volume of quenching buffer (6 M Gn·HCl, 200 mM NaH_2PO_4, 100 mM TCEP, pH 7.0), diluted with 1 ml of CH_3CN/H_2O/AcOH (47.5:47.5:5, vol/vol/vol), and further purified by preparative HPLC (10 to 50 solvent B over 30 min, Proto-300 C4 column) to yield protein **10** (3.7 mg, yield 86%). Under the same conditions, peptide hydrazine **15** (1.6 mg, 5 equiv.) was reacted with protein **8** (3.0 mg, 1 equiv.) to afford protein **16** (3.1 mg, yield 93%). The resulting proteins **10** and **16** were analysed by LC-MS. To convert C1166 to native alanine, 2 mg of protein **10** or **16** was dissolved in 200 µl of desulfurization buffer (6 M Gn·HCl, 200 mM NaH_2PO_4, pH 7.0) under an argon atmosphere, to which 200 µl of 0.5 M bond-breaker TCEP solution, 20 µl of 2-methyl-2-propanethiol and 100 µl of radical initiator were added. The reaction mixture was gently stirred at 37 °C for 48 h. On completion, the reaction was diluted with 1 ml of CH_3CN/H_2O/AcOH (47.5:47.5:5, vol/vol/vol) and purified by preparative HPLC (32 to 36% solvent B over 30 min, Proto-300 C4 column) to yield SynGAP-S1159^{OG} (protein **11**, 1.1 mg, 55% yield) and SynGAP CC-PBM (EPL-N, protein **17**, 0.8 mg, 40% yield). The resulting proteins **11** and **17** were analysed by LC-MS.

Matrix-assisted laser desorption ionization time-of-flight mass spectrometry analysis. The semisynthetic proteins **6**, **11**, **14** and **17** in acetonitrile/water (1:1, vol/vol) solution at 50 µM were mixed with an equal volume of 20 mg ml^{-1} sinapinic acid matrix solution and spotted to the matrix-assisted laser desorption ionization (MALDI) target plate (1 µl). After drying, the samples were analysed on an AB SCIEX TOF/TOF 5800 (AB SCIEX, USA) instrument using the positive and linear mode with a UV nitrogen laser (337 nm), an accelerating potential of 12 kV and an extraction delay of 730 ns.

Folding of semisynthetic proteins. After lyophilization, protein **6**, **11**, **14** or **17** was dissolved in freshly prepared denaturing buffer (20 mM Tris-HCl, 500 mM NaCl, 10 mM DTT, 5% glycerol, 8 M urea, pH 7.5) with gentle sonication. The solution was gently stirred by gradient dialysis against urea at decreasing concentrations from 8 M to 0 M at 4 °C and finally changed with phase separation assay buffer (50 mM Tris-HCl pH 7.8, 100 mM NaCl, 1 mM EDTA and 5 mM DTT). The solution was then centrifuged at 18,407*g* at 4 °C for 15 min to remove aggregates. The supernatant was collected, concentrated by 3-kDa Amicon Ultra centrifugal filter devices (Millipore), and the concentration was determined by a NanoDrop 2000c system (Thermo Fisher Scientific).

To prepare partially *O*-GlcNAylated SynGAP CC-PBM, recombinant SynGAP CC-PBM was purified on a preparative HPLC (20–60% solvent B gradient over 30 min, Proto-300 C4 column), followed by lyophilization. The lyophilized SynGAP CC-PBM and SynGAP T1306^{OG} proteins were separately dissolved in denaturing buffer with gentle sonication. The protein concentrations were determined using a NanoDrop 2000c instrument. Two solutions were mixed together to give the designated molar ratios. The mixed solutions were dialysed against urea at decreasing concentrations to refold as described above.

Circular dichroism. CD spectra of 2.5 µM proteins in 10 mM PBS buffer (pH 7.4) were recorded on a JASCO J-815 spectrometer from 310 nm to 180 nm at r.t. in a quartz cell with 1-mm path length. The spectra measurements were performed in triplicate, subtracted from the blank, and smoothed and averaged to yield a final spectrum for each sample.

In vitro LLPS assays. For the sedimentation assay, the SynGAP protein (recombinant, semisynthetic or partially *O*-GlcNAcylated) was mixed with PSD-95 at a molar ratio of 1:1 (unless otherwise specified) at the indicated concentrations in phase separation assay buffer at r.t. for 10 min. The samples were centrifuged at 18,000*g* for 10 min at 20 °C on a benchtop temperature-controlled microcentrifuge. The supernatants and pellets were separated into different tubes immediately after centrifugation. Each pellet was resuspended in phase separation assay buffer with the same volume of the corresponding supernatant. The fractions were then resolved on 12.5% or precast 4–20% SDS–PAGE gels and stained with CBB. Band intensities were quantified by ImageJ/Fiji.

For imaging LLPS in vitro, the protein samples were mixed and immediately injected into a home-made chamber with a glass coverslip bottom, and sealed to prevent evaporation, followed by time-lapse DIC and/or fluorescence microcopy on a Zeiss LSM700 confocal microscope using a ×63/1.40 oil objective lens. Where needed, PSD-95 contained 1% TAMRA-conjugated protein. To conjugate PSD-95 with TAMRA, the protein was exchanged into freshly prepared $NaHCO_3$ buffer (100 mM $NaHCO_3$, pH 8.3, 150 mM NaCl, 1 mM EDTA, 2 mM DTT) and concentrated to 5–10 mg ml^{-1}. 5-Carboxy-tetramethylrhodamine *N*-succinimidyl ester (5-TAMRA, Sigma) in DMSO was added at the fluorophore to a protein molar ratio of 3:1 and incubated at r.t. for 1 h. The reaction was quenched by adding 200 mM Tris-HCl (pH 8.0) and further purified by desalting column (GE Healthcare). ImageJ/Fiji and MATLAB were used for imaging processing. For quantification of the liquid droplet area, at least nine images (resolution of 1,024 × 1,024) of randomly selected fields were acquired for each sample. Each sample was imaged for three independent replicates. The images were exported to the Tiff format using the ZEN software. The liquid droplet area of each image was quantified using MATLAB. In brief, images were transformed to greyscale images using the Rgb2gray function. The edge detection operator was then applied to define the droplet boundary. The total pixel number within the boundary (droplet pixel number) was calculated with Imdilate and Imfill function processing. The droplet pixel number was then divided by the total pixel number of the image to give the droplet area percentage of each image. The droplet area percentage values of each sample were averaged and presented as mean ± s.d.

FRAP assay. The FRAP assay was performed on a Zeiss LSM700 confocal microscope equipped with a ×63/1.4 oil objective lens at r.t. For the in vitro FRAP assay, with the selected droplets of >10-µm diameter, a spot of ~5-µm diameter was irradiated using a 555-nm solid-state laser to bleach the PSD-95 PSG (1% labelled with TAMRA). Recovery of the fluorescence after photo-bleaching was recorded every 5 s for 10 min. The fluorescence intensity was scaled between 100% (the intensity before photo-bleaching) and 0% (intensity immediately after photo-bleaching). For the FRAP assay of PSD-95 PSG/SynGAP CC-PBM LLPS in living cells, HEK293T cells were cultured in eight-well chamber slides and transfected as described above. The GFP signal was bleached using a 488-nm solid-state laser. Puncta with a diameter of 0.5–1.5 µm were assayed. Recovery of the fluorescence intensity after photo-bleaching was recorded every 8 s for 5 min.

Size-exclusion chromatography coupled with static light scattering. The size-exclusion chromatography coupled with static light scattering assay was performed on an AKTA FPLC system (GE Healthcare) coupled with a static light

scattering detector (miniDawn, Wyatt) and a differential refractive index detector (Optilab, Wyatt). The proteins (50 μM) in the buffer (50 mM Tris-HCl pH 8.3, 100 mM NaCl, 1 mM EDTA, 2 mM DTT) were filtered and loaded into a Superose 12 10/300 GL column (GE Healthcare) pre-equilibrated by the same buffer. Data were processed with the ASTRA6 software (Wyatt).

ITC assay. ITC measurements were performed on a MicroCal ITC200 calorimeter at 25 °C. To 400 μl of 20 μM PSD-95 in titration buffer (10 mM PBS buffer, pH 7.5, 5 mM TCEP) in the sample cell was added 0.5 μl of 200 μM pep or OG-pep for the first titration point, followed by 2-μl additions for the following titration points using syringe injection. A total of 18 injections were performed with a time interval of 150 s. ITC titration data were analysed using Origin9.2 software and fitted with the one-site binding model.

Inhibition of LLPS by SynGAP peptides. For in vitro inhibition, 100 μM SynGAP CC-PBM and PSD-95 PSG were mixed and injected into a home-made chamber, and the pep or OG-pep stock solution was added to reach a final concentration of 600 μM. The SynGAP CC-PBM and PSD-95 PSG concentrations were minimally altered. Time-lapse microscopy was performed to monitor LLPS.

For inhibition in living cells, HEK293T cells expressing GFP-SynGAP CC-PBM and RFP-PSD-95 PSG cultured in 35-mm glass-bottom culture dishes were exchanged with customized Tyrode's buffer (10 mM HEPES, pH 7.3, 125 mM NaCl, 2.5 mM KCl, 3 mM $CaCl_2$, 1 mM $MgCl_2$, 30 mM glucose). The buffer was adjusted to 305–310 mOsm kg^{-1} with sucrose (extracellular medium). The whole-cell patch-clamp recording was performed at r.t. Borosilicate glass electrodes (Sutter) were pulled to a tip resistance of 2.5–5 MΩ, and recordings were terminated if the membrane resistance changed by >10%. The glass electrode was filled with internal solution (10 mM HEPES, pH 7.3, 125 mM potassium gluconate, 8 mM NaCl, 0.6 mM $MgCl_2$, 0.1 mM $CaCl_2$, 1 mM EGTA, 4 mM Mg-ATP, 0.4 mM Na-GTP) and adjusted to 295 mOsm kg^{-1} with 1 M sucrose. For peptide delivery, 1 mM pep or OG-pep and 0.1 mM Cascade Blue-conjugated dextran (3 kDa, as a fluorescent marker of peptide delivery, D7132, Thermo Fisher) were dissolved into the internal solution on ice and loaded into the glass electrode. The glass electrode's position was adjusted by a Sutter MP285 micromanipulator, and the whole-cell patch-clamp-based injection was established after a gigaseal and performed in voltage-clamp mode with a −30-mV holding potential using an Axopatch 200B amplifier (Axon Instruments). After rupturing the membrane by applying negative pressure, 20-min time-lapsed (5 min per frame) fluorescence imaging of Cascade Blue (405-nm excitation), GFP-SynGAP CC-PBM (488-nm excitation) and RFP-PSD-95 PSG (561-nm excitation) was performed on an inverted fluorescence microscope (Nikon-TiE) equipped with a ×40/1.3 oil immersion objective lens at 2 × 2 camera binning with an exposure time of 50–200 ms in Z-stack mode with a 0.4–0.6-μm step length (that is, 15–30 layers in a stack of the entire cell). The images were processed with ImageJ/Fiji and a custom software written by MATLAB (MathWorks, version R2016b). The size of the puncta in the time-lapsed imaging sequence was determined by the voxels affiliated to the puncta in the corresponding image stacks. For every stack, image-by-image thresholding (150–300% of the mean fluorescence intensity of the entire cell) was performed to select puncta-affiliated voxels. The total fluorescence intensity of the puncta-affiliated voxels was considered as the fluorescence intensity of the puncta. The cells with severe deformation, motion blur or with bad delivery efficiency (monitored by the fluorescence increment of Cascade Blue in time-lapse imaging) were excluded from the analysis.

OGA- and OGT-mediated LLPS. *E. coli* cells expressing His_6-OGA were collected, resuspended in binding buffer, lysed and purified by nickel affinity purification as described above. The OGA protein was further purified by gel filtration on a Superdex 200 column (GE Healthcare) in enzyme-mediated LLPS assay buffer (25 mM HEPES pH 7.5, 150 mM NaCl, 1 mM EDTA, 5 mM DTT). For OGA-mediated LLPS assay, semisynthetic SynGAP-$T1306^{OG}$ protein alone or with PSD-95 was treated with 10 μM OGA in OGA assay buffer for 4 h at r.t. The resulting mixtures were subjected to Y298L GalT1-based chemoenzymatic analysis or an in vitro phase separation assay in OGA assay buffer.

The OGT protein was expressed and purified following the same procedures. For the OGT-mediated LLPS assay, SynGAP in enzyme-mediated LLPS assay buffer was incubated with 10 μM OGT, 5 mM UDP-GlcNAc (or as indicated) at 37 °C for 4 h or at r.t. overnight. The resulting samples were subjected to the in vitro phase separation assay and Y298L GalT1-based analysis.

Statistics. GraphPad Prism 6.0, Origin 9.2 and Microsoft Excel 2019 were used for statistics. For quantification assays in this Article, typically three or more independent experiments (numbers of independent batches of experiments are given in the figures when more than three times) were used to derive final data. Statistic data are represented as mean ± s.d. For the box-and-whiskers plot, the horizontal lines mark the maximum, median and minimum values of the data, and boxes mark upper and lower quartiles. For comparison between groups, one-way ANOVA with Tukey's multiple comparisons test or with Dunnett's multiple comparisons test was used to determine differences.

Reporting summary. Further information on research design is available in the Nature Research Reporting Summary linked to this Article.

Data availability

All relevant data presented in this study are provided in the Article, Extended Data figures and Supplementary Information. The data and genetic constructs are also available from the corresponding authors upon request. The crystal structure of the PSD-95 PDZ3-C/SynGAP PBM complex is from https://www.rcsb.org/structure/5JXB (PDB 5JXB). Source data are provided with this paper.

Code availability

MATLAB code can be downloaded from GitHub at https://github.com/XChenlab/LLPS. Alternatively, it is available from the corresponding authors upon request.

Acknowledgements

We thank Y. Liu for help with the Rosetta simulation. Parts of the MS experiments were performed at the Analytical Instrumentation Center of Peking University (PKUAIC). This work was supported by the National Key R&D Program of China (no. 2018YFA0507600 to X.C., S.D., C.L. and P.Z.) and the National Natural Science Foundation of China (nos. 91753206 and 21521003 to X.C. and no. 21708002 to W.Z.).

Author contributions

X.C. conceived the study and supervised the entire project. X.C., P.L. and Y.D. designed the experiments and analysed the data. P.L. and Y.D. performed most of the experiments, unless otherwise specified, with the help of X.Z., Y.W., M. Zeng, L.P., W.Z., P.Z., C.L. and M. Zhang. C.H. performed the protein semisynthesis under the supervision of S.D. The manuscript was written by X.C., P.L. and Y.D., with input from all the authors.

Competing interests

The authors declare no competing interests.

Additional information

Extended data is available for this paper at https://doi.org/10.1038/s41557-022-00946-9.

Supplementary information The online version contains supplementary material available at https://doi.org/10.1038/s41557-022-00946-9.

Correspondence and requests for materials should be addressed to Suwei Dong or Xing Chen.

Peer review information *Nature Chemistry* thanks Xiaoyong Yang and the other, anonymous, reviewer(s) for their contribution to the peer review of this work.

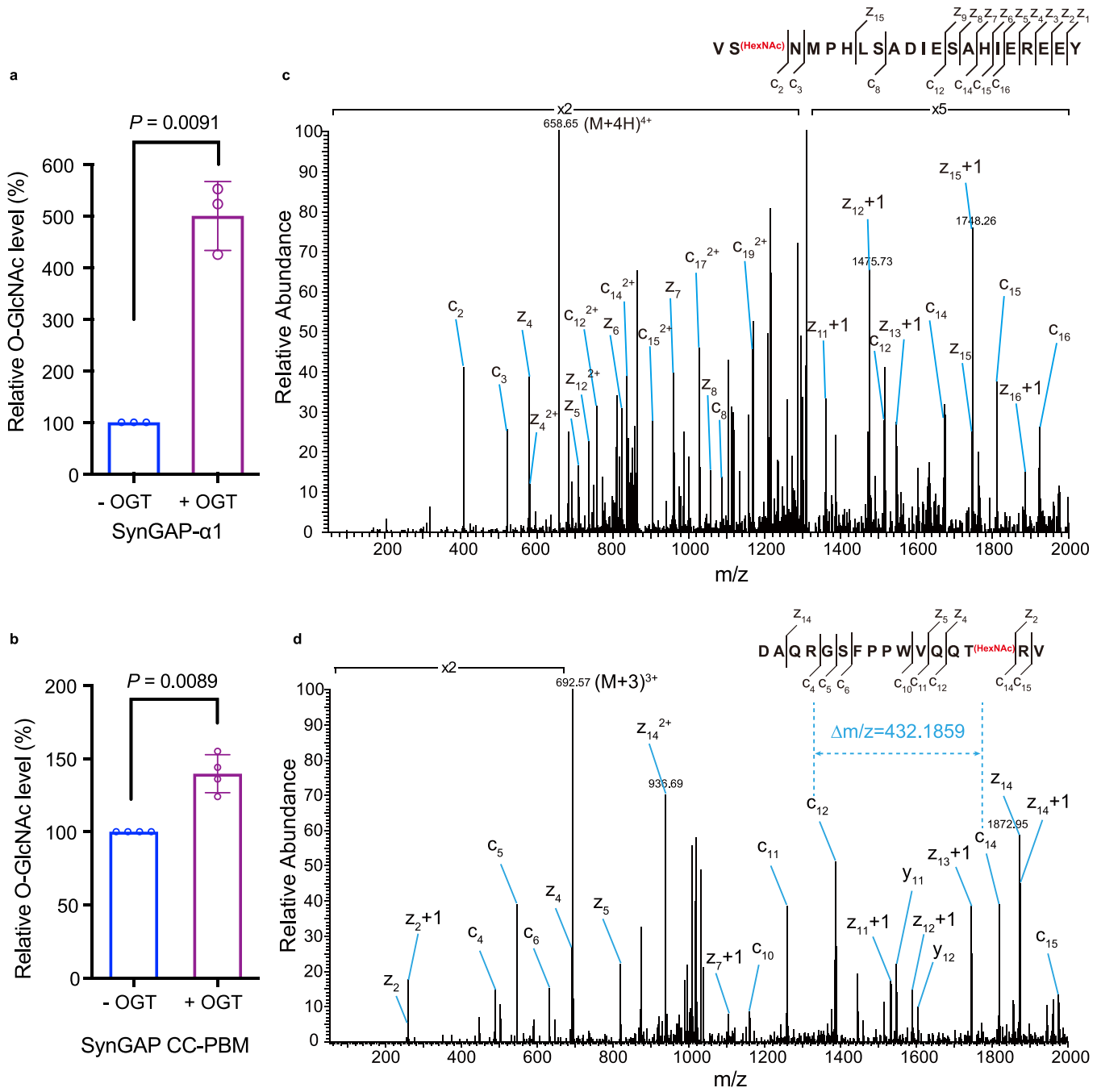

Extended Data Fig. 1 | O-GlcNAcylation of SynGAP. a,b, Bar graph showing relative O-GlcNAcylation levels in Fig. 1c (**a**) and Fig. 1d (**b**). In **a** and **b**, the relative O-GlcNAcylation levels are normalized to that of GFP-SynGAP-α1 with no OGT overexpression and that of GFP-SynGAP CC-PBM with no OGT overexpression, respectively. Error bars represent mean ± SD. Results are from three independent experiments. Unpaired two-tailed Student's t-test with 95% CI was used to determine difference, $p < 0.05$ is considered significant. **c,d**, ETD-MS/MS spectra of two O-GlcNAcylated peptides of recombinant GFP-SynGAP CC-PBM purified from HEK293T co-expressing OGT. The c_2 ion unambiguously confirms O-GlcNAcylation at S1159 (**c**). The c_{12} and c_{14} ions unambiguously confirms O-GlcNAcylation at T1306 (**d**). The matched fragment ions are marked.

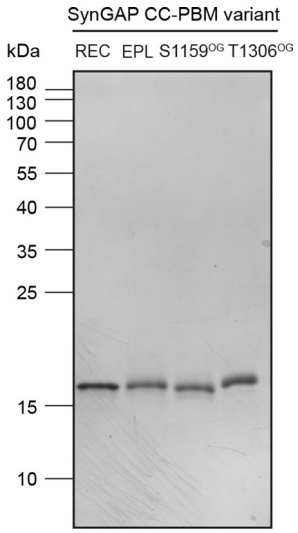

Extended Data Fig. 2 | SDS PAGE analysis of recombinant SynGAP CC-PBM, EPL-synthesized SynGAP CC-PBM, SynGAP-S1159^{OG}, and SynGAP-T1306^{OG}. SynGAP-T1306^{OG} exhibited a slightly higher molecular weight than SynGAP-S1159^{OG}, which can be attributed to the four residual amino acids at the N-terminus of SynGAP-T1306^{OG}. The recombinant and EPL-synthesized SynGAP CC-PBM shown here contain the four amino acids. Of note, the four residual amino acids do not affect the LLPS behaviour of SynGAP CC-PBM/PSD-95 PSG (data not shown). Representative results are shown from three independent experiments.

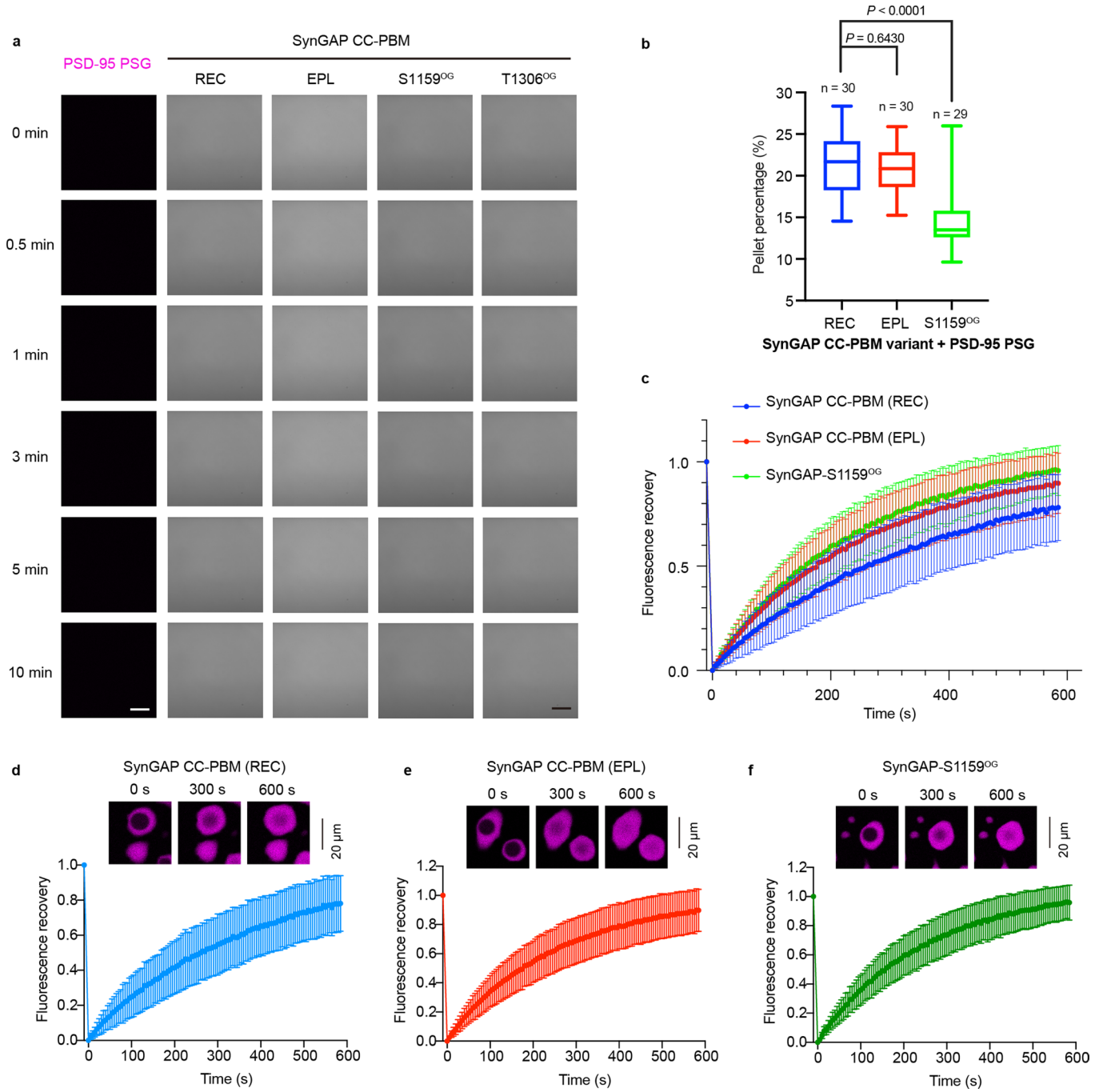

Extended Data Fig. 3 | Quantification and FRAP analysis of liquid droplets imaging of SynGAP proteins with PSD-95. a, Time-lapse images of the PSD-95 PSG or SynGAP CC-PBM protein alone (80 μM PSD-95 PSG with 1% conjugated with TAMRA fluorophore, fluorescence channel; 80 μM SynGAP CC-PBM variants, DIC channel). Under the same experimental conditions as Fig. 2g, no liquid droplet was observed, indicating that PSD-95 PSG or SynGAP CC-PBM alone cannot undergo LLPS. Scale bar, 10 μm. **b**, Box-and-whiskers plot showing statistical analysis of the liquid droplet areas of Fig. 2g. The horizontal lines mark the maximum, median and minimum values of the data, and boxes mark upper and lower quartiles. For each group, at least 30 fluorescence images from at least three independent experiments were analysed. Differences were assessed by one-way ANOVA followed by Tukey's multiple comparisons test with 95% CI, and $p < 0.05$ is considered significant. **c-f**, Recovery of PSD-95 PSG fluorescence over time after photo-bleaching a small region with the droplet of the complex of PSD-95 PSG (with 1% conjugated with TAMRA) with recombinant SynGAP CC-PBM (**d**), EPL-synthesized SynGAP CC-PBM (**e**), or SynGAP-S1159^{OG}(**f**). The overlayed FRAP curves are shown in **c**. The results are from at least three independent experiments and represented as mean ± SD.

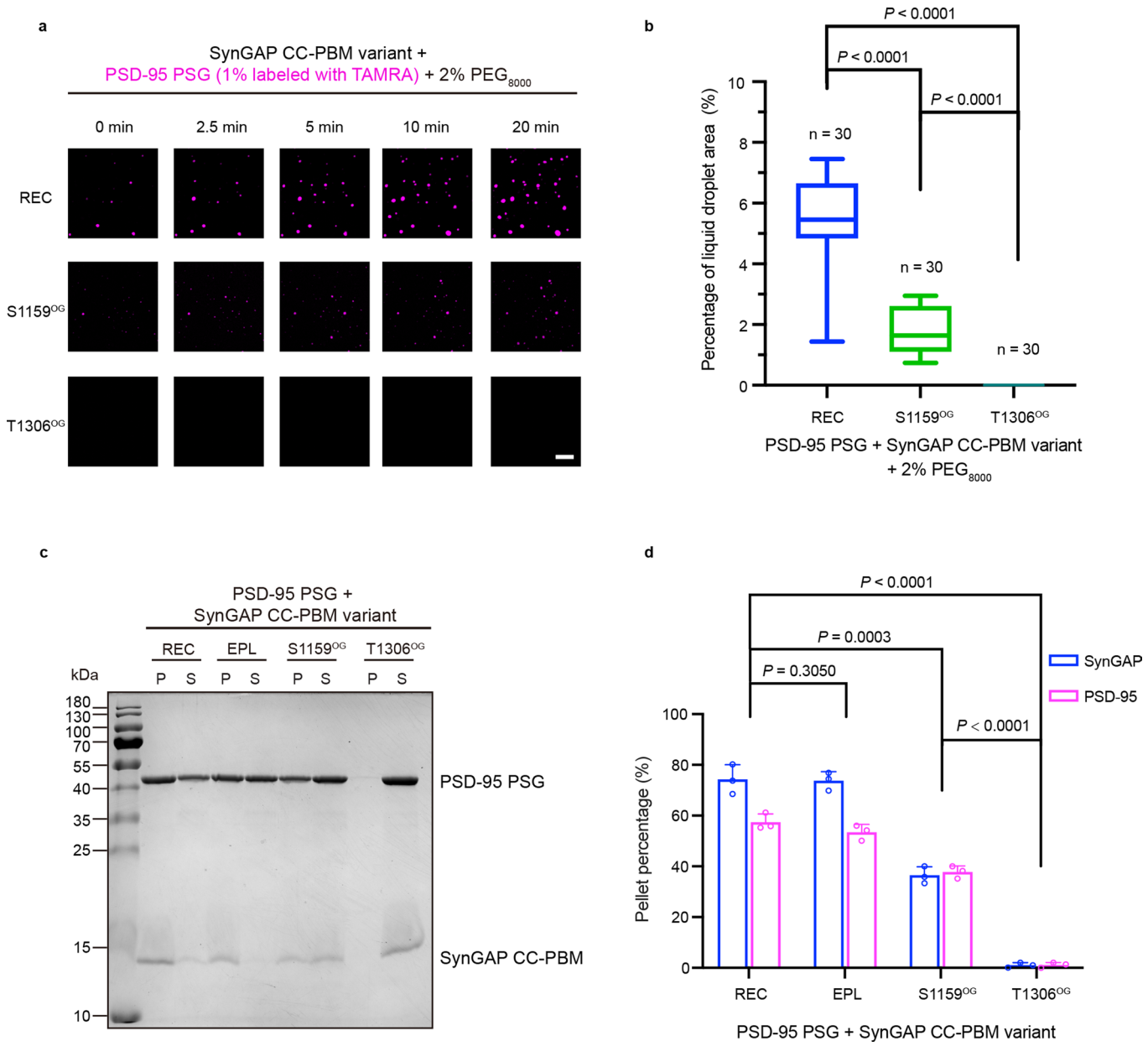

Extended Data Fig. 4 | LLPS of the mixtures of PSD-95 PSG with different SynGAP CC-PBM proteins at the physiological concentration. a, Time-lapse fluorescence images showing LLPS of 5 μM PSD-95 PSG and recombinant SynGAP CC-PBM, semisynthetic SynGAP CC-PBM, SynGAP-S1159^{OG}, or SynGAP-T1306^{OG}, with 2% PEG_{8000} over 20 min. Scale bar, 10 μm. **b**, Box-and-whiskers plot shows statistical analysis of the liquid droplet areas of **a**. The horizontal lines mark the maximum, median and minimum values of the data, and boxes mark upper and lower quartiles. For each group, at least 30 fluorescence images from at least three independent experiments were analysed. Differences were assessed by one-way ANOVA followed by Tukey's multiple comparisons test with 95% CI, $p < 0.05$ is considered significant. **c**, SDS-PAGE gel showing the distributions of PSD-95 and SynGAP proteins in the supernatant (S) and pellet (P) in the sedimentation-based assay. 5 μM PSD-95 or SynGAP proteins were mixed for 10 min at r.t. in the presence of the crowding reagent (2% PEG_{8000}) and subjected with the sedimentation-based assays. Bar graph on the right shows quantification of the distributions. **d**, Bar graph shows quantification results in **a**. The quantification results are from three independent experiments and represented as mean ± SD. Differences were assessed by one-way ANOVA followed by Tukey's multiple comparisons test with 95% CI, $p < 0.05$ is considered significant.

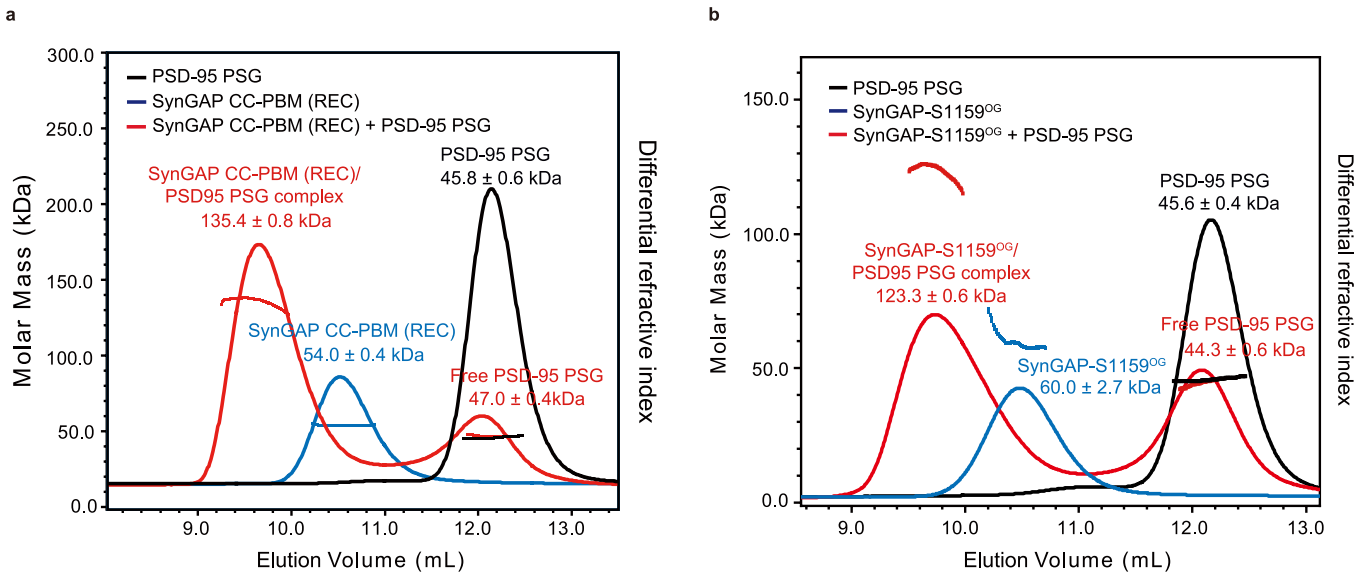

Extended Data Fig. 5 | SEC-SLC analysis of complex formation. a, Curves showing PSD-95 PSG, SynGAP CC-PBM, and the 1:1 mixture of PSD-95 PSG and SynGAP CC-PBM. **b**, Curves showing PSD-95 PSG, SynGAP-S1159^{OG}, and the 1:1 mixture of PSD-95 PSG and SynGAP-S1159^{OG}.

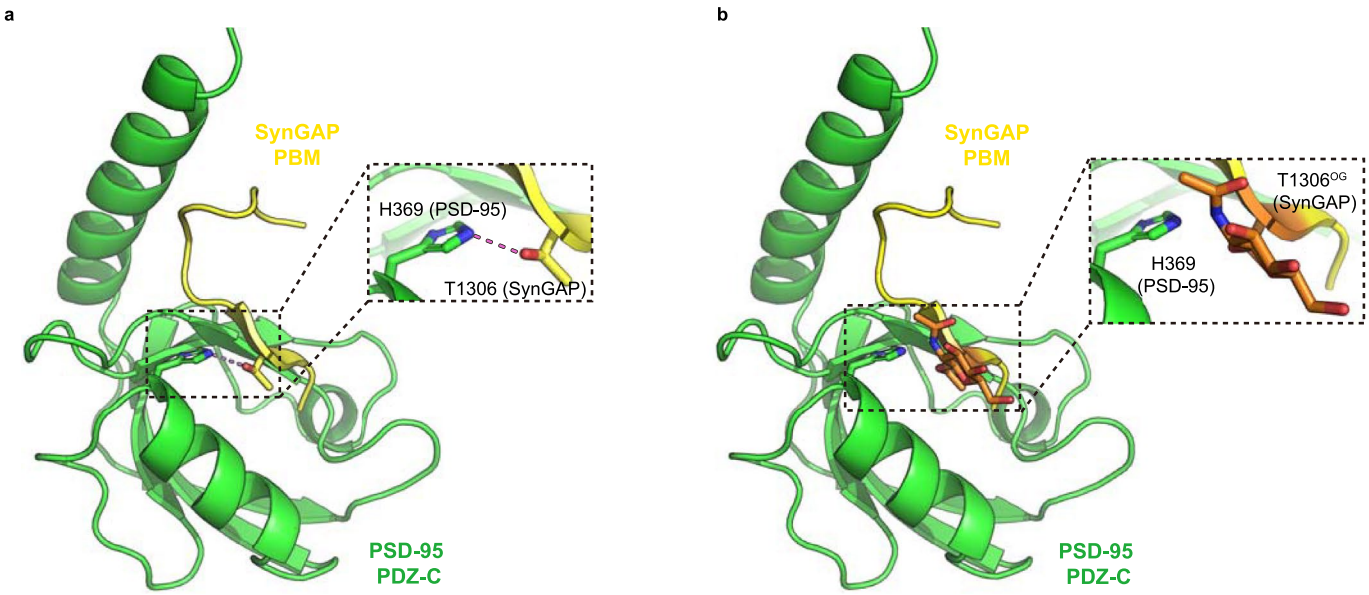

Extended Data Fig. 6 | 3D structural modelling of the SynGAP PBM-T1306^{OG}/PSD-95 PDZ3-C complex. a, Crystal structure of the PSD-95 PDZ3-C/SynGAP PBM complex (PDB code: 5JXB). The zoomed-in view shows the interaction between PSD-95 H369 and SynGAP T1306. **b**, Modelled structure of the PSD-95 PDZ3-C/SynGAP PBM-T1306OG based on the PSD-95 PDZ3-C/SynGAP PBM structure by using Rosseta homology modeling. The zoomed-in view shows that the interaction between PSD-95 H369 and SynGAP T1306 is blocked by the O-GlcNAc moiety. Note that the crystal structure and the modeled structure were obtained with SynGAP PBM fused to PSD-95 PDZ3-C with a flexible linker. The linker holds SynGAP PBM in close proximity to PSD-95 PDZ3-C even when T1306 O-GlcNAc disrupts the interaction.

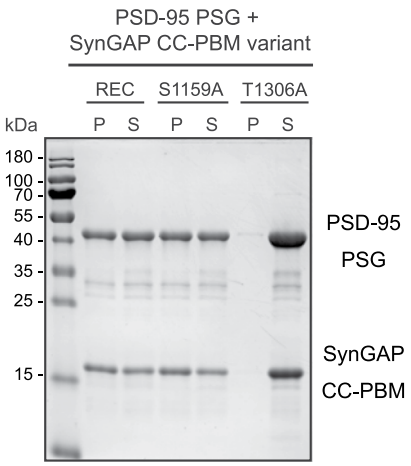

Extended Data Fig. 7 | SDS-PAGE gel showing the distribution of SynGAP CC-PBM, SynGAP CC-PBM-S1159A and SynGAP-T1306A in the supernatant (S) and pellet (P) when mixed with PSD-95 PSG in sedimentation assay. 80 μM PSD-95 and SynGAP CC-PBM variant were mixed for 10 min at r.t. and then subjected to the sedimentation-based assay. Representative results are shown from three independent experiments.

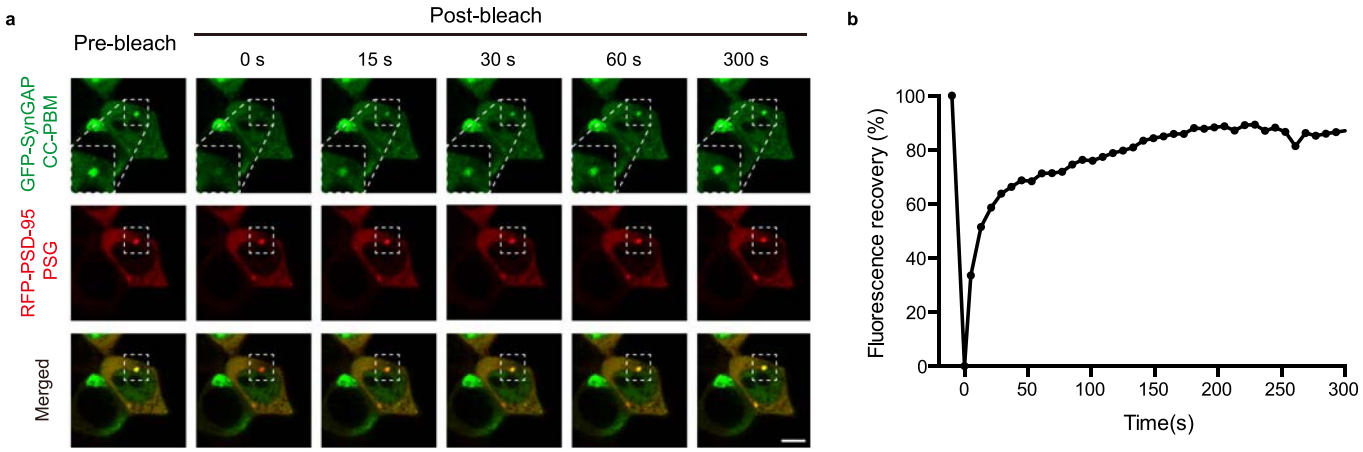

Extended Data Fig. 8 | FRAP analysis of LLPS of GFP-SynGAP/RFP-PSD-95 in living cells. a, Representative time-lapse fluorescence images showing the recovery of GFP-SynGAP fluorescence in a punctum over a few minutes. The fluorescence of GFP was selectively bleached at 0 s and the RFP fluorescence remained unchanged. Scale bar: 5 μm. Representative results are shown from three independent experiments. **b**, Quantification of the recovery of GFP-SynGAP fluorescence over time in the punctum shown in **a**.

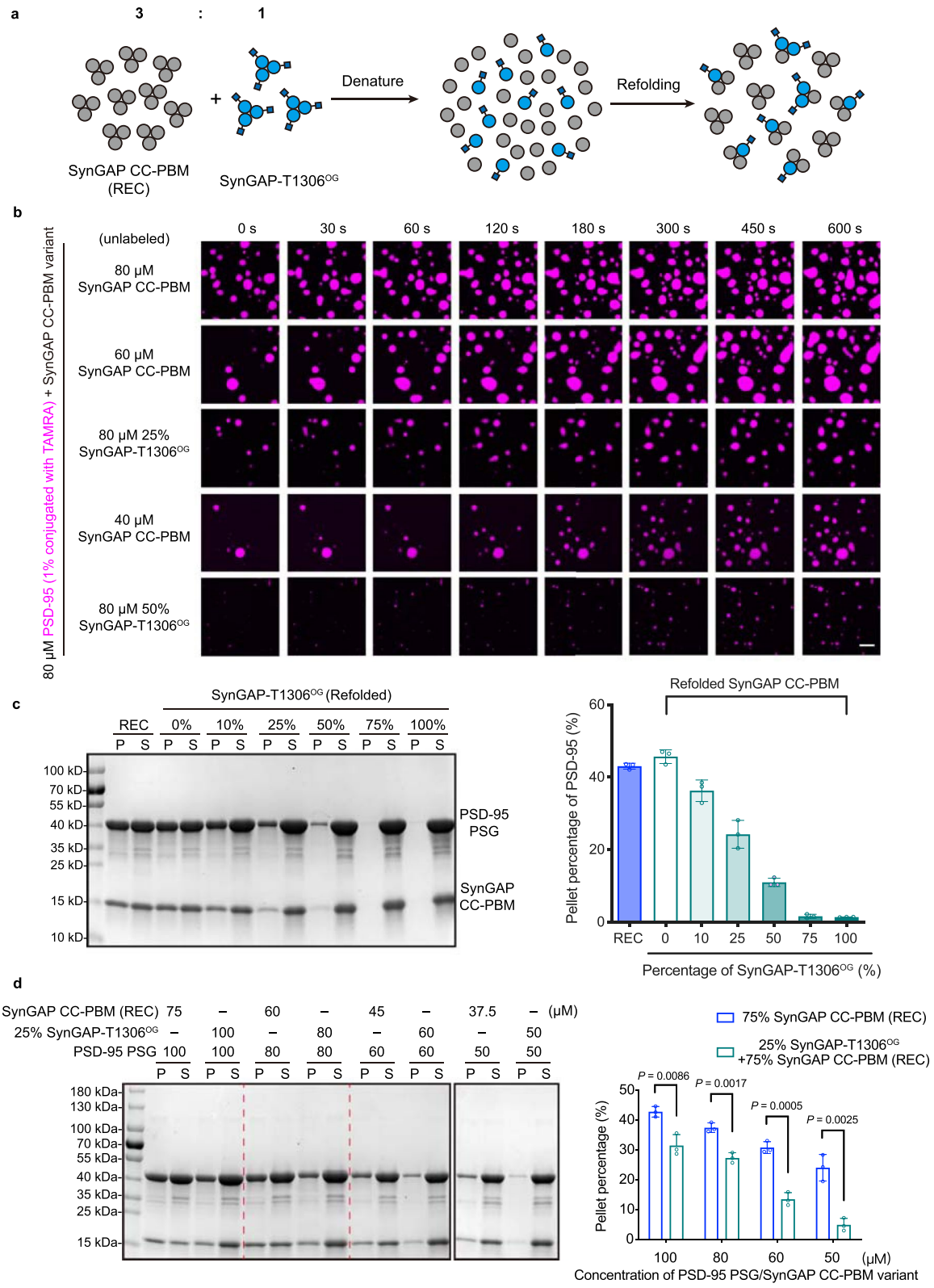

Extended Data Fig. 9 | See next page for caption.

Extended Data Fig. 9 | Dominant-negative effect of SynGAP T1306 O-GlcNAcylation on LLPS of PSD-95 PSG/SynGAP CC-PBM. a, Schematic showing the procedures for forming the overall 25% O-GlcNAcylated SynGAP CC-PBM trimers with no, one, two, and three O-GlcNAc at the ratio of 42.2%:42.2%:14.0%:1.6%. **b**, Time-lapse fluorescence images showing LLPS of PSD-95 PSG with SynGAP CC-PBM at indicated concentrations and O-GlcNAcylated ratios over 10 min. Scale bar, 10 μm. **c**, SDS-PAGE gel showing the distributions of SynGAP CC-PBM and PSD-95 PSG in the supernatant (S) and pellet (P). 80 μM PSD-95 PSG were mixed with 80 μM partially O-GlcNAylated SynGAP CC-PBM with varied O-GlcNAcylation stoichiometry ranging from 10% to 100%. **d**, SDS-PAGE gel showing the distribution of SynGAP CC-PBM and PSD-95 PSG in the supernatant (S) and pellet (P). PSD-95 PSG at varied concentrations was mixed with SynGAP CC-PBM or 25% O-GlcNAcylated SynGAP CC-PBM at indicated concentrations. Unpaired two-tailed Student's t-test with 95% CI was used to determine difference, $p < 0.05$ is considered significant. In **c** and **d**, bar graphs showing quantification of the distributions. The quantification results were represented as mean ± SD. In **b-d**, representative results are shown from three independent experiments.

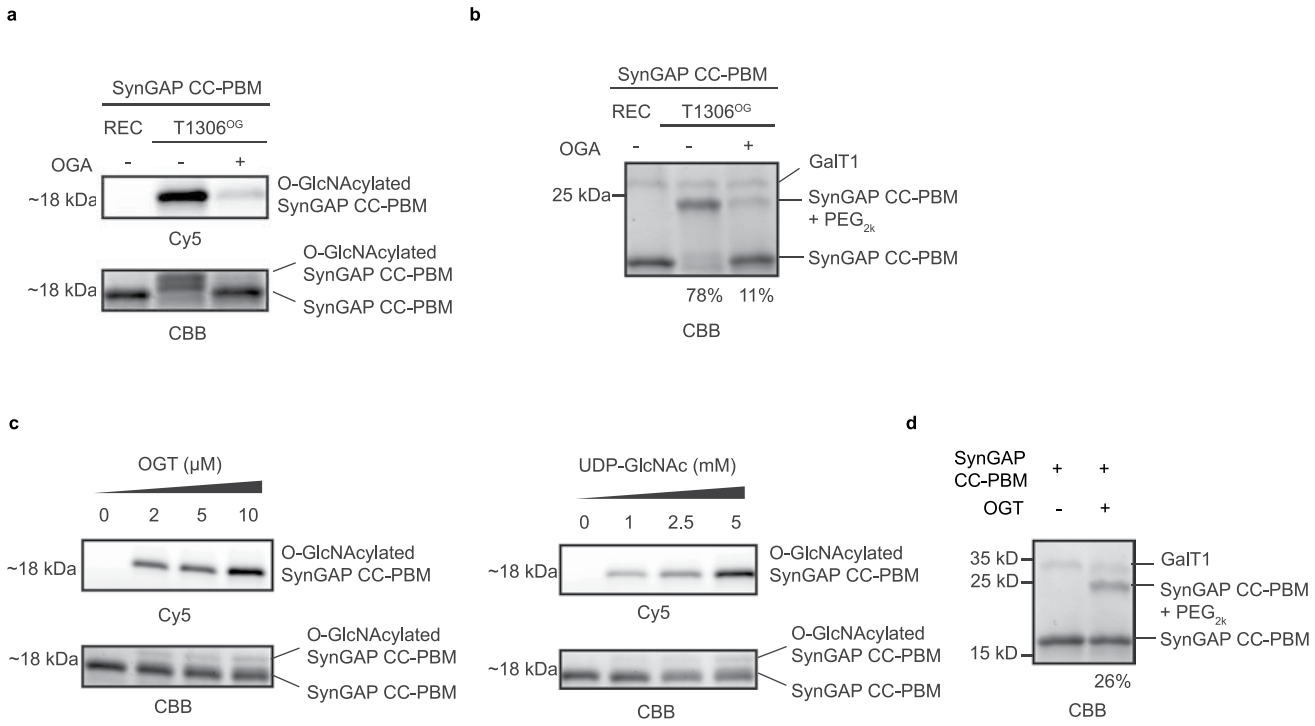

Extended Data Fig. 10 | OGA and OGT treatment of SynGAP-T1306^{OG} and SynGAP. a, Representative in-gel fluorescence scanning showing O-GlcNAcylation of SynGAP CC-PBM, SynGAP-T1306^{OG}, and SynGAP-T1306^{OG} treated with 10 μM OGA at r.t. for 4 h. The proteins were incubated with Y289L GalT1 and UDP-GalNAz, reacted with alkyne-Cy5. **b**, SDS-PAGE gel showing the O-GlcNAcylation levels of SynGAP CC-PBM, SynGAP-T1306^{OG}, and SynGAP-T1306^{OG} treated with 10 μM OGA for 4 h. The proteins were incubated with Y298L GalT1 and UDP-GalNAz, and reacted with alkyne-PEG$_{2k}$. Note that SynGAP CC-PBM was non-O-GlcNAcylated. The calculated stoichiometry was shown below the gel. Incomplete GalT1-based enzymatic reaction and click reaction could contribute to the apparent stoichiometry. Nevertheless, OGA treatment removed the majority of O-GlcNAc from SynGAP-T1306^{OG}. **c**, In-gel fluorescence scanning showing SynGAP CC-PBM incubated with OGT at varied concentrations and 5 mM UDP-GlcNAc (left panel) or with 10 μM OGT and UDP-GlcNAc at varied concentrations (right panel) overnight. **d**, SDS-PAGE gel showing the O-GlcNAcylation levels of SynGAP incubated with 10 μM OGT and 5 mM UDP-GlcNAc overnight. After OGT treatment, the proteins were incubated with Y298L GalT1 and UDP-GalNAz, and reacted with alkyne-PEG$_{2k}$. The calculated stoichiometry was shown below the gels. In **a** and **c**, coomassie brilliant blue (CBB)-stained gels were shown as the loading control. In a-d, representative results are shown from three independent experiments.

nature research

Corresponding author(s): Xing Chen and Suwei Dong

Last updated by author(s): Feb 9, 2022

Reporting Summary

Nature Research wishes to improve the reproducibility of the work that we publish. This form provides structure for consistency and transparency in reporting. For further information on Nature Research policies, see our Editorial Policies and the Editorial Policy Checklist.

Statistics

For all statistical analyses, confirm that the following items are present in the figure legend, table legend, main text, or Methods section.

n/a	Confirmed	
☐	☒	The exact sample size (*n*) for each experimental group/condition, given as a discrete number and unit of measurement
☐	☒	A statement on whether measurements were taken from distinct samples or whether the same sample was measured repeatedly
☐	☒	The statistical test(s) used AND whether they are one- or two-sided *Only common tests should be described solely by name; describe more complex techniques in the Methods section.*
☒	☐	A description of all covariates tested
☐	☒	A description of any assumptions or corrections, such as tests of normality and adjustment for multiple comparisons
☐	☒	A full description of the statistical parameters including central tendency (e.g. means) or other basic estimates (e.g. regression coefficient) AND variation (e.g. standard deviation) or associated estimates of uncertainty (e.g. confidence intervals)
☐	☒	For null hypothesis testing, the test statistic (e.g. *F*, *t*, *r*) with confidence intervals, effect sizes, degrees of freedom and *P* value noted *Give P values as exact values whenever suitable.*
☒	☐	For Bayesian analysis, information on the choice of priors and Markov chain Monte Carlo settings
☒	☐	For hierarchical and complex designs, identification of the appropriate level for tests and full reporting of outcomes
☒	☐	Estimates of effect sizes (e.g. Cohen's *d*, Pearson's *r*), indicating how they were calculated

Our web collection on statistics for biologists contains articles on many of the points above.

Software and code

Policy information about availability of computer code

Data collection	The LC-MS/MS data were obtained from Thermo Xcalibur 2.2 SP1.48. The UV-Vis chromatograms of analytical LC-MS were acquired from Waters 2489 UV/Visible detector, and the MS spectra of analytical LC-MS were acquired from Waters SQD mass spectrometry. The MALDI-TOF-MS analyses were carried out on an AB SCIEX TOF/TOFTM 5800 (AB SCIEX, USA) instrument. The protein concentrations were determined by NanoDrop 2000c. CD spectra were recorded on a JASCO J-815 spectrometer. The SEC-SLC assays were performed on an AKTA FPLC system (GE Healthcare) coupled with a static light scattering detector (miniDawn, Wyatt) and a differential refractive index detector (Optilab, Wyatt). The ITC measurements were performed on a MicroCal ITC200 calorimeter. FRAP assays and in vitro LLPS imaging were performed on a Zeiss LSM 700 confocal microscope. Intracellular peptide delivery was conducted using an Axopatch 200B amplifier (Axon Instruments) and Z-stack time-series imaging was performed on an inverted fluorescence microscope (Nikon-TiE) equipped with a spinning disk confocal unit (Yokogawa CSU-X1). In-gel fluorescence scanning was conducted from a Typhoon FLA 9500 (GE Healthcare). Images of Coomassie Brilliant Blue-stained gels were collected on a ChemiDoc XRS+ (Bio-Rad). Western blotting and streptavidin blotting were acquired from a Tanon-5200Multi (Tanon) and ChemiDoc XRS+ (Bio-Rad).
Data analysis	GraphPad Prism 6.0, Origin 9.2 and Microsoft Excel 2019 for statistics. ImageLab (version 5.2.1), Image J/Fiji (version 1.52a), MATLAB (version R2016b) and ZEN 2012 for image analysis. Mascot (version 2.3.02, MatrixScience) for database searches. MassLynx (version 4.1) for LC-MS deconvolution. The SEC-SLC Data were processed with ASTRA6 software (Wyatt).

For manuscripts utilizing custom algorithms or software that are central to the research but not yet described in published literature, software must be made available to editors and reviewers. We strongly encourage code deposition in a community repository (e.g. GitHub). See the Nature Research guidelines for submitting code & software for further information.

Data

Policy information about availability of data

All manuscripts must include a data availability statement. This statement should provide the following information, where applicable:

- Accession codes, unique identifiers, or web links for publicly available datasets
- A list of figures that have associated raw data
- A description of any restrictions on data availability

All relevant data presented in this study are provided in the Article, Extended Data figures and Supplementary Information. MATLAB code can be downloaded from GitHub at https://github.com/XChenlab/LLPS. The data and genetic constructs are also available from the corresponding authors upon request. Crystal structure of the PSD-95 PDZ3-C/SynGAP PBM complex was from https://www.rcsb.org/structure/5JXB (PDB code: 5JXB). Source data are provided with this paper.

Field-specific reporting

Please select the one below that is the best fit for your research. If you are not sure, read the appropriate sections before making your selection.

☒ Life sciences ☐ Behavioural & social sciences ☐ Ecological, evolutionary & environmental sciences

For a reference copy of the document with all sections, see nature.com/documents/nr-reporting-summary-flat.pdf

Life sciences study design

All studies must disclose on these points even when the disclosure is negative.

Sample size	In general, the experimental analysis was performed in at least three independent replicates and standard error of the experimental data was calculated. For quantification of the liquid droplet area, at least 27 samples/images were collected from at least three independent replicates. For intracellular peptide delivery, more than 15 samples/cells were recorded from at lest three independent replicates.
Data exclusions	No data were excluded from the analyses.
Replication	At least three biological replicates.
Randomization	Randomization is not relevant, because independent experiments such as immunoblotting and in-gel fluorescence scanning cannot be randomized.
Blinding	For imaging related assays, data were unbiasedly collected and analysed by Pinou Lv, Yifei Du and Luxin Peng.

Reporting for specific materials, systems and methods

We require information from authors about some types of materials, experimental systems and methods used in many studies. Here, indicate whether each material, system or method listed is relevant to your study. If you are not sure if a list item applies to your research, read the appropriate section before selecting a response.

Materials & experimental systems

n/a	Involved in the study
☐	☒ Antibodies
☐	☒ Eukaryotic cell lines
☒	☐ Palaeontology and archaeology
☐	☒ Animals and other organisms
☒	☐ Human research participants
☒	☐ Clinical data
☒	☐ Dual use research of concern

Methods

n/a	Involved in the study
☒	☐ ChIP-seq
☒	☐ Flow cytometry
☒	☐ MRI-based neuroimaging

Antibodies

Antibodies used	Primary antibodies included anti-SynGAP (Rb, Abcam, ab3344, 1: 1000); anti-GFP (Rb, Abcam, ab32146, 1: 10000); anti-FLAG (Ms, BioLegend, 637301, 1: 5000); anti-O-GlcNAc CTD110.6 (Ms, Santa Cruz, sc-59623, 1: 200); anti-GAPDH-HRP (Ms, Abcam, ab9482, 1: 5000). Secondary antibodies included goat anti-mouse IgG H&L HRP (Abcam, ab6789, 1: 5000), goat anti-rabbit IgG H&L HRP (Abcam, ab6721, 1: 5000), goat anti-mouse IgM HRP (Invitrogen, 31440, 1: 5000).
Validation	All antibodies are validated by vendors indicated above. Anti-SynGAP antibody (ab3344) reacts with rat and human SynGAP, and tested for ICC/IF, IHC-P application. Anti-GFP antibody (ab32146) is species independent, and tested for ICC/IF, IP application. Anti-FLAG antibody (Bioledend 637301) reacts with DYKDDDDK tag epitope, and tested for IP, ICC, ELISA, FC, purification application. Anti-O-GlcNAc CTD110.6 antibody (sc-59623) is

used to detect Ser-O-GlcNAc and Thr-O-GlcNAc in a broad range of species including including mammals, insects, worms, plants and filamentous fungi by Western Blotting and IP application. Anti-GAPDH-HRP antibody (ab9482) reacts with mouse, rat, human GAPDH, and tested for WB application.

Eukaryotic cell lines

Policy information about cell lines

Cell line source(s)	HEK293T cells were obtained from ATCC (ATCC CRL-11268).
Authentication	No further authentication was performed.
Mycoplasma contamination	The cells were tested negative for mycoplasma contamination.
Commonly misidentified lines (See ICLAC register)	None.

Animals and other organisms

Policy information about studies involving animals; ARRIVE guidelines recommended for reporting animal research

Laboratory animals	4-week old male Sprague-Dawley rats were ordered from Charles River Laboratories. Rat-related experiments were conducted in accordance with institutional guidelines.
Wild animals	No wild animals were involved in this study.
Field-collected samples	No field-collected samples involved in this study.
Ethics oversight	Beijing Laboratory Animal Research Center (BLARC). All animal experiments were performed in accordance with guidelines approved by the Institutional Animal Care and Use Committee of Peking University accredited by AAALAC International.

Note that full information on the approval of the study protocol must also be provided in the manuscript.